Molecular Biology of the Cell
Vol. 15, 4695–4709, October 2004

NrCAM Coupling to the Cytoskeleton Depends on Multiple Protein Domains and Partitioning into Lipid Rafts

Julien Falk,* Olivier Thoumine,† Caroline Dequidt,† Daniel Choquet,† and Catherine Faivre-Sarrailh‡§

*Neurogenèse et Morphogenèse du Développement à l'Adulte, UMR 6156 CNRS, Institut de Biologie du Développement de Marseille, Marseille, France; †Physiologie Cellulaire de la Synapse, UMR 5091 CNRS, Institut François Magendie, Université Bordeaux 2, France; and ‡Neurobiologie des Interactions Cellulaires et Neurophysiopathologie, UMR 6184 CNRS, Institut Jean-Roche, Marseille, France

Submitted March 2, 2004; Revised July 5, 2004; Accepted July 6, 2004
Monitoring Editor: Richard Hynes

NrCAM is a cell adhesion molecule of the L1 family that is implicated in the control of axonal growth. Adhesive contacts may promote advance of the growth cone by triggering the coupling of membrane receptors with the F-actin retrograde flow. We sought to understand the mechanisms leading to clutching the F-actin at the site of ligand-mediated clustering of NrCAM. Using optical tweezers and single particle tracking of beads coated with the ligand TAG-1, we analyzed the mobility of NrCAM-deletion mutants transfected in a neuroblastoma cell line. Deletion of the cytoplasmic tail did not prevent the coupling of NrCAM to the actin flow. An additional deletion of the FNIII domains to remove *cis*-interactions, was necessary to abolish the rearward movement of TAG-1 beads, which instead switched to a stationary behavior. Next, we showed that the actin-dependent retrograde movement of NrCAM required partitioning into lipid rafts as indicated by cholesterol depletion experiments using methyl-β-cyclodextrin. Recruitment of the raft component caveolin-1 was induced at the adhesive contact between the cell surface and TAG-1 beads, indicating that enlarged rafts were generated. Photobleaching experiments showed that the lateral mobility of NrCAM increased with raft dispersion in these contact areas, further suggesting that TAG-1–coated beads induced the coalescence of lipid rafts. In conclusion, we propose that anchoring of NrCAM with the retrograde actin flow can be triggered by adhesive contacts via cooperative processes including interactions with the cytoplasmic tail, formation of *cis*-complex via the FNIII repeats, and lipid raft aggregation.

INTRODUCTION

Cell adhesion molecules of the immunoglobulin superfamily (IgCAMs) are major players in the control of axonal growth and guidance. NrCAM is a transmembrane molecule that contains both Ig and fibronectin type III (FNIII) domains and belongs to the L1-family of IgCAMs also including L1, CHL1, and neurofascin. In vitro studies have indicated that NrCAM participates to diverse combinatorial associations of IgCAMs and extracellular matrix molecules that finely tune axonal growth. NrCAM mediates homophilic binding and heterophilic interactions with F3/contactin, TAG-1, neurofascin, RPTPβ/z (Volkmer *et al.*, 1996; Sakurai *et al.*, 1997; Zacharias *et al.*, 1999). NrCAM has been involved in the axogenesis of different neuronal populations acting both as a ligand and a receptor. It is implicated in the control of sensory axon patterning and in the midline crossing of commissural axons in the spinal cord of chick embryo (Stoeckli and Landmesser, 1995; Perrin *et al.*, 2001). NrCAM acts as a functional receptor for F3/contactin to regulate axonal outgrowth of cerebellar neurons (Faivre-Sarrailh *et al.*, 1999; Sakurai *et al.*, 2001; Falk *et al.*, 2002). NrCAM-deficient mice do not display any gross morphological alteration, but double knock-out mice for L1 and NrCAM exhibit severe defects in cerebellar morphogenesis, indicating that the two molecules may have overlapping functions (Sakurai *et al.*, 2001).

The growth cone is the sensor and motor device on which the trajectory of the growing axon relies. Growth cone motility depends on the dynamics of actin filaments, generated by actin polymerization at the leading edge and myosin-dependent rearward flow of F-actin. Extension or retraction of the growth cone results from a balance between these two opposing processes that appear to be independently regulated by environmental cues (Lin and Forscher, 1995; Jay, 2000). Substrate-bound cues may promote advance of the growth cone by physically anchoring membrane receptors with the actin retrograde flow, thereby generating tension forces needed to pull the growth cone forward. This was first evidenced in neurons for the *Aplysia* homologue of NCAM, ApCAM (Suter *et al.*, 1998). Coupling of IgCAMs with the actin flow has been also established for NrCAM (Faivre-Sarrailh *et al.*, 1999) and L1 (Kamiguchi and Yoshihara, 2001). Such linkage between IgCAMs and the actin filaments may consist in a general transductory mechanism for axonal guidance and has been also evidenced for other classes of membrane receptors, the β1-integrin and N-cadherin (Schmidt *et al.*, 1995; Grabham *et al.*, 2000; Lambert *et al.*, 2002). The question arises of whether distinct types of adap-

Article published online ahead of print. Mol. Biol. Cell 10.1091/mbc.E04–03–0171. Article and publication date are available at www.molbiolcell.org/cgi/doi/10.1091/mbc.E04–03–0171.

§ Corresponding author. E-mail address: sarrailh.c@jean-roche.univ-mrs.fr.

tors mediate the recruitment of F-actin by the different families of membrane receptors.

Several motifs of interactions with the cytoskeleton have been identified that are conserved in L1-type molecules. The ankyrin-binding motif has been extensively characterized (Bennett and Chen, 2001) and association with ankyrin-G is essential for the targeting of NrCAM and neurofascin at the node of Ranvier. On the contrary, ankyrin binding does not seem to be a key element for the coupling of L1 with the retrograde actin flow in growth cones. Ankyrin-B440 is only distributed in the proximal region of the growth cone (Kunimoto, 1995; Nishimura *et al.*, 2003), and ankyrin binding has been shown to inhibit retrograde movement of L1 and to mediate a stationary behavior (Gil *et al.*, 2003). The juxtamembrane domain of L1-molecules has been shown to confer association of L1 with the actin cytoskeleton (Dahlin-Huppe *et al.*, 1997). NrCAM also contains a C-terminal PDZ-domain–binding motif. Thus, different domains of the NrCAM cytoplasmic tail can account for the coupling with the actin flow. In addition, *cis*-interactions between L1-molecules and other transmembrane receptors have been reported (Brümmendorf and Rathjen, 1996). For example, L1-CAM clustering on the cell surface has been shown to induce its homomultimerization and recruitment of integrins via interaction with the FNIII domains (Silletti *et al.*, 2000).

By tracking the movement of microspheres coated with F3/contactin, we previously demonstrated that NrCAM displays an actin-dependent retrograde mobility on the growth cones of cerebellar granule cells (Faivre-Sarrailh *et al.*, 1999). Here, our goal was to further investigate the mechanisms underlying the membrane mobility of NrCAM and its anchorage to the actin cytoskeleton.

MATERIALS AND METHODS

Constructs

The rat NrCAM12 cDNA is a kind gift of V. Bennett. The HA epitope was inserted by PCR 5 amino acids (aa) downstream of the signal peptide in NrCAM12 subcloned in pIRES1neo (Clontech, Palo Alto, CA). The amino acids of NrCAM12 were numbered as in Davis *et al.* (1996). A construct with deletion of the cytoplasmic tail (NrCAMΔcyt) was generated by introducing a STOP codon at position 1042. NrCAM-GFP chimeras were generated using pEGFP-C1 (Clontech). The NrCAMΔfn construct, in which the FNIII domains were replaced by the GFP, was generated by PCR amplification of the signal peptide and Ig domain sequence (aa −30–607) and insertion in *Nhe*I-*Age*I sites upstream of the GFP coding sequence in pEGFP-C1. Next, the transmembrane and cytoplasmic domains (aa 999-1154) were amplified by PCR and inserted in the *Xho*I-*Bam*HI sites of the polylinker. Alternatively, the NrCAMΔfnΔcyt construct was obtained by PCR amplification of the transmembrane domain (aa 999-1041) and insertion in *Xho*I-*Bam*HI. The NrCAMΔfnΔCter was obtained by PCR amplification of the transmembrane domain and part of the cytoplasmic tail (aa 999-1084) and insertion in *Xho*I-*Bam*HI. The GFP-TM construct was generated by insertion of the signal peptide of NrCAM (aa −30–16) in *Nhe*I-*Age*I sites upstream of GFP and insertion of the transmembrane domain (aa 999-1041) in *Xho*I-*Bam*HI. The PCR-amplified products were verified by sequencing (Genome Express, Meylan, France).

Antibodies

A recombinant protein was generated using the pQE30 vector (Qiagen, Courtaboeuf, France), which carried a his-tag fused to Ig2–6 domains of rat NrCAM12. After induction, the his-NrCAM fusion protein was purified under denaturing conditions by affinity chromatography on Ni-agarose beads and used for the immunization of rabbits. Rabbit anti-ezrin was a gift from Dr. P. Mangeat. Rabbit anti-GFP antibody and rat anti-HA (3F10) mAb were purchased from Roche (Meylan, France). Rabbit and mouse anti-human Fc, mouse IgM anti–α-actinin, and mouse IgG anti-talin were from Sigma (Saint-Quentin Fallavier, France) and rabbit anti-caveolin-1 from Calbiochem (La Jolla, CA). Alexa 488–conjugated secondary antibodies were purchased from Molecular Probes (Eugene, OR). Peroxidase- and Texas red–conjugated secondary antibodies were from Jackson ImmunoResearch (West Grove, PA).

Cell Culture

B104 cells were grown in DMEM medium with 10% FCS. B104 cells were transfected using Lipofectamine Plus (Invitrogen, Carlsbad, CA) with NrCAM, NrCAMΔcyt, NrCAMΔfn, NrCAMΔfnΔcyt, NrCAMΔfnΔCter, or GFP-TM constructs. After 2 weeks of selection with G418, stable lines expressing the different constructs were selected using immunofluorescence for HA, fluorescence of GFP, or binding of the TAG-1IgFc chimera clustered with anti-Fc antibodies.

Cell Extracts and Western Blot

Transfected cells were lyzed for 30 min on ice with 50 mM Tris, pH 7.5, 1% Triton X-100, containing 10 mM $MgCl_2$ and protease inhibitors and then centrifuged at 4°C for 15 min at 15,000 rpm. Cell lysates were analyzed by 7% SDS-PAGE and Western blotting with rabbit anti-NrCAM immune serum (1:1000) or anti-HA mAb (1:1000) and peroxidase-conjugated secondary antibodies using chemiluminescence detection kit (Roche).

Low-density Lubrol-insoluble complexes were prepared as previously described (Faivre-Sarrailh *et al.*, 2000). B104 cells (10^7) were lyzed in 2 ml of 25 mM MES, pH 6.5, containing 0.15 M NaCl, 1% Lubrol, and protease inhibitors. The extract adjusted to 40% sucrose was placed at the bottom of a 5–30% linear sucrose gradient and centrifuged at 4°C for 17 h at 39,000 rpm in a SW41 Beckman rotor (Fullerton, CA). Fractions (1 ml) were collected and analyzed by 7% SDS-PAGE and immunoblotting for NrCAM constructs using anti-HA or anti-GFP mAb, and for caveolin-1 and α-actinin.

Fc-chimera and Bead Preparation

NrCAMFc, F3Fc, and TAG-1IgFc chimeras were previously described (Faivre-Sarrailh *et al.*, 1999; Pavlou *et al.*, 2002). The chimeras produced in eukaryotic cells were immunoadsorbed on mouse or rabbit anti-human Fc-coupled latex sulfate beads of 1-μm (Polysciences, Niles, IL) or 4-μm (Frontier Bioscience, Interfacial Dynamics, Portland, OR) diameter as described previously (Faivre-Sarrailh *et al.*, 1999). For concanavalin-A (con-A) coating, carboxylated beads (Polysciences) were covalently coupled to biotinylated BSA, incubated with Neutravidin (Molecular Probes), and then with biotinylated con-A (Sigma) as described (Choquet *et al.*, 1997).

Videomicroscopy, Single-particle Tracking, and Laser Trapping

Cells were plated on poly-L-lysine coated glass coverslips (10 μg/ml for 1 h at 37°C) the day before the experiment. To enhance cell motility, cells were serum-starved for 1 h before being mounted in an observation chamber with DMEM, 1% BSA, and 20 mM HEPES containing diluted TAG-1 beads. When indicated, 2 μM cytochalasin D, 10 mM methyl-β-cyclodextrin (MBCD), or a mixture of cholesterol and MBCD at a molar ratio of 1:6 (Kenworthy *et al.*, 2004) was added to the medium at this point. The optical setup consisted of an inverted microscope (Olympus IX 70, Tokyo, Japan) fed through its epifluorescence port by a Nd:YAG laser beam (Compass 1064 nm, Coherent, Palo Alto, CA), reflected by a dichroic mirror (Chroma, Rockingham, VT) and focused by a 100×/1.45 NA oil objective (Zeiss, Le Pecq, France). The beam power was adjusted at 150 mW (we measured ~10 μW at the front of the objective, which is small enough not to harm the cells). Microbeads were trapped with the laser beam and manipulated using a motorized stage (MarzHauser, Wetzlar, Germany), and digital images were acquired with DIC illumination using a cooled CCD camera (HQ Cool Snap, Roper Scientific, Evry, France). Beads were placed for 5 s in the peripheral region of cell lamellipodia. Behavior of the beads was observed for 1 min after initial attachment and classified as rearward moving or not. Resistance to the laser trap was also tested on each bead, by placing the trap ~0.5 μm behind the bead, where the trap force is maximal (Choquet *et al.*, 1997). In some experiments nonrearward moving beads were further characterized as diffusing or stationary (if bead displacements did not exceed 1 μm during the 1-min period of observation). Alternatively, bead mobility was recorded at a 40-ms rate for the 90 s after attachment. Bead displacement was followed using the tracking object application of Metamorph software (Universal Imaging Corp, Downington, PA). The mean squared displacement (MSD) was calculated using a homemade software and fitted by the equation $4Dt + V^2t^2$, where t is the time, D the diffusion coefficient, and V the directed velocity (Choquet *et al.*, 1997).

Fluorescence Recovery after Photobleaching

The fluorescence recovery after photobleaching (FRAP) setup used the same microscope together with a 488-nm beam from an argon laser (Innova 300, Coherent). The laser beam is expanded to fill out the pupil of a 100×/1.4 NA objective and adjusted via a translatable lens to yield a diffraction-limited spot on the focal plane. The laser power was set to 150 mW, corresponding to 80 μW at the front of the objective. Wide-field illumination was achieved via a regular Xenon lamp, deported at 90° and joining the optical path via a 70/30 beamsplitter (Chroma). Both the lamp and laser illuminations were controlled by shutters. A region of interest was brought to the position of the laser spot and the FRAP sequence was started: a few reference images were acquired

first, and then the sample was bleached by the laser for 2 s, and fluorescence recovery was recorded for 5 min. Images were acquired with a CCD camera with exposure times of 50–200 ms. The whole sequence was driven by a journal written in the Metamorph software. Four FRAP sequences were run per coverslip, bringing the experiment duration to ~30 min. Using cells fixed with paraformaldehyde, we measured the diameter of the bleached area (~4 μm for a 2-s exposure at full laser power) and the photobleaching due to the illumination sequence itself (<5%).

Immunofluorescence Staining and Bead-cell Adhesion Assays

MBCD Treatment and Triton X-100 Extraction. Cells were rinsed with serum-free culture medium for 2 h, treated or not with 10 mM MBCD for 30 min, and then incubated with rabbit anti-GFP antibody at 4°C for 30 min. Thereafter, cells were incubated with 0.1% Triton X-100 at 4°C for 3 min, fixed with formaldehyde 4% in PBS for 10 min, and incubated with Texas red–conjugated anti-rabbit immunoglobulins. Incubation with filipin (50 μg/ml) was carried out to detect cholesterol and epifluorescence was done with an UV filter as described in Marchand *et al.* (2002).

Bead-cell Adhesion Assays. NrCAM- or NrCAMΔfnΔcyt-expressing B104 cells were treated or not with 10 mM MBCD for 30 min and incubated with TAG-1–conjugated beads (4-μm diameter) for 30 min. Cells fixed with 4% paraformaldehyde were permeabilized with Triton X-100 and processed for immunofluorescence staining with anti-caveolin-1 (1:500), anti-ezrin (1:2000), anti–α-actinin (1:200), or anti-talin (1:200) and Texas red–conjugated anti-rabbit IgG, anti-mouse IgG or anti-mouse IgM, or staining using Texas red–conjugated phalloidin (Molecular Probes). Alternatively, cells were incubated with TAG-1 beads (4 μm) for 15 min and treated or not with 10 mM MBCD for an additional period of 15 min. Then, a quantitative analysis of GFP-fluorescence clusters of NrCAMΔfnΔcyt recruited under the beads was performed on more then 50 cells under each condition and two perpendicular diameters were measured for each GFP cluster using the Metamorph software.

RESULTS

Specificity of Binding between TAG-1 Beads and NrCAM-transfected Cells

Because primary neuronal cultures endogenously express several L1-type molecules, we turned to a simplified cellular model, a rat neuroblastoma B104 cell line (Garver *et al.*, 1997), which does not express endogenous NrCAM (Figure 1B). We established stable lines of B104 cells transfected with full-length NrCAM or several deleted forms of the molecule: deletion of the cytoplasmic tail (NrCAMΔcyt); deletion of the FNIII repeats, which were replaced by GFP (NrCAMΔfn); and deletions of both the FNIII repeats and cytoplasmic tail (NrCAMΔfnΔcyt) or C-terminal region of the cytoplasmic tail (NrCAMΔfnΔCter; Figure 1A). A construct that contains the signal peptide of NrCAM upstream and the transmembrane region of NrCAM downstream of GFP was generated for control experiments (Figure 1A). All constructs were tagged with an HA epitope at the N-terminus. The selected lines transfected with full-length NrCAM or deleted constructs produced similar levels of recombinant protein as analyzed by Western blotting with anti-HA mAb (Figure 1B). Immunofluorescence staining for the HA epitope indicated that all the deletion mutants of NrCAM were expressed at the cell surface (unpublished data).

Because parental B104 cells displayed binding sites for F3/contactin (Figure 1E), we decided to use TAG-1 as another physiological ligand to trigger the coupling of NrCAM to the cytoskeleton. However, TAG-1 displays a strong homophilic binding activity essentially mediated by its FNIII repeats (Tsiotra *et al.*, 1996) that results in the stable aggregation of TAG-1Fc chimera. To favor heterophilic binding, we used a construct deleted from the FNIII repeats (TAG-1IgFc) that has been previously characterized for its strong interaction with NrCAM (Pavlou *et al.*, 2002). Beads coated with the chimera TAG-1IgFc (hereafter abbreviated TAG-1), selectively bound to NrCAM-expressing cells, whereas no significant binding was observed on parental B104 cells (Figure 1, C–E). In addition, the binding sites for soluble TAG-1 were colocalized with the receptor NrCAM expressed at the membrane as illustrated with the NrCAMΔfnΔcyt construct containing the GFP sequence (Figure 1, F–H).

Actin-dependent Retrograde Mobility of TAG-1 Beads on the Surface of NrCAM-transfected B104 Cells

On differentiation in serum-free medium, B104 cells exhibited neurites and growth cone-like projections. We took advantage of the well-defined actin retrograde flow in these motile structures (Lin and Forscher, 1995) to study NrCAM coupling with the actin cytoskeleton. We analyzed the strength of NrCAM anchorage to the cytoskeleton using laser tweezers (Figure 2). TAG-1 beads were trapped and maintained for 5 s at the periphery of lamellipodial structures of differentiated NrCAM-expressing B104 cells. This resulted in stable attachment of the beads to the cell surface (83%, n = 35), and no bead release was observed during the 3-min period after the trap release (Figure 2A). As controls, <20% of TAG-1 beads attached on the parental or GFP-TM–expressing B104 cells (Figure 2A). The major part of the bound TAG-1 beads (80%, n = 65) instantaneously adopted a rearward movement on the lamellipodia away from the leading edge with a mean directional velocity of 2.4 ± 0.4 μm/min (n = 9; Figure 2, B and C; Table 1). The MSD vs. time followed a parabolic curve characteristic of a unidirectional mobility and plotting of X and Y coordinates showed a uniform bead movement over time (Figure 2C). A similar velocity has been recorded for NrCAM on the growth cones of cerebellar granule cells in our previous time-lapse study (Faivre-Sarrailh *et al.*, 1999), and for other CAMs (Kamiguchi and Yoshihara, 2001; Lambert *et al.*, 2002) and corresponds to the velocity of the F-actin rearward flow. To directly demonstrate the implication of F-actin in the rearward movement, cells were treated with 2 μM cytochalasin D, a drug which depolymerizes actin filaments. This treatment abolished the retrograde mobility of most TAG-1 beads positioned on NrCAM-expressing cells. Instead, the beads adopted a stationary behavior (86%, n = 23) and the MSD curves indicated a reduced mean directional velocity of 0.5 ± 0.2 μm/min (n = 4; Figure 2, B and D). Such stationary behavior of NrCAM receptors may depend on their association with a cortical actin cytoskeleton resistant to depolymerization. To test this hypothesis, the laser trap was placed ~0.5 μm behind the bead (where the trap force is maximal) trying to displace the bead. Indeed, most TAG-1 beads were resistant to displacement by the laser trap in the presence of cytochalasin D (77%, n = 21; Table 1), suggesting that the receptors were anchored to some static elements.

Deletion of the Cytoplasmic Tail of NrCAM Does Not Abrogate the Retrograde Mobility of TAG-1 Beads

We postulated that the coupling of NrCAM to the actin retrograde flow may rely on its cytoplasmic domain because several motifs of interaction with the cytoskeleton have been identified (Figure 1A). To analyze the role of the cytoplasmic tail, a truncated form of NrCAM (NrCAMΔcyt) with only two residues remaining in the cytoplasmic domain was stably expressed in B104 cells. Selected clones expressing the same amount of full-length and deleted NrCAM were used in laser trapping experiments (Figure 1B). TAG-1 beads attached well to NrCAMΔcyt-expressing cells (95%, n = 84). Most of the

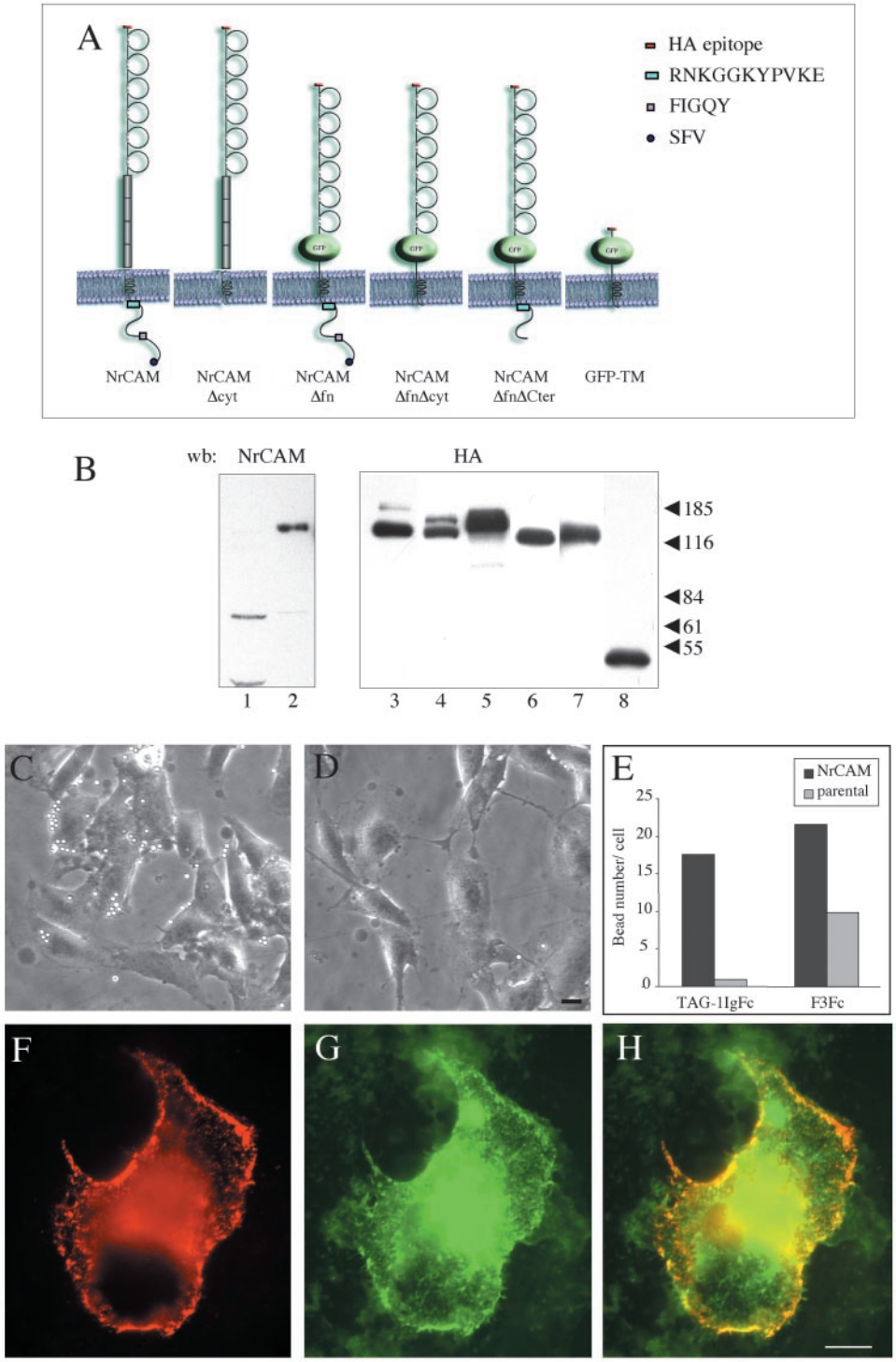

Figure 1. Expression of full-length NrCAM and deleted constructs in neuroblastoma B104 cells. (A) Schematic representation of the different NrCAM expression constructs. All constructs were tagged with a HA epitope inserted 5 aa downstream of the signal peptide. NrCAMΔcyt is deleted from the cytoplasmic region. NrCAMΔfn is deleted from the 4 FNIII repeats that are replaced by GFP, NrCAMΔfnΔcyt displays an additional deletion of the cytoplasmic tail and NrCAMΔfnΔCter of the C-terminal region of the cytoplasmic tail. GFP-TM contains the signal peptide of NrCAM upstream and the transmembrane region of NrCAM downstream of GFP. Motifs of interaction with the cytoskeleton are indicated including a juxta-membrane domain (RNKGGKYPVKE) corresponding to a consensus sequence for the binding of FERM adaptors, the FIGQY ankyrin-binding motif, and a SFV C-terminal PDZ-domain binding motif. (B) Expression of NrCAM and deleted constructs in stably transfected B104 cell lines. Cells were lysed with Triton X-100 and analyzed by SDS-PAGE and Western blotting with anti-NrCAM (lanes 1 and 2) or anti-HA antibodies (lanes 3–8). NrCAM is not detected in the lysate from parental B104 cells (lane 1) and is detected at 130 kDa in the NrCAM-expressing line (lanes 2 and 3). NrCAMΔcyt (lane 4), NrCAMΔfn (lane 5), NrCAMΔfnΔcyt (lane 6), and NrCAMΔfnΔCter (lane 7) are detected with an apparent M_r higher than the calculated molecular mass of 115, 112, 99, and 103, respectively, likely due to glycosylation. GFP-TM (lane 8) is detected at 31 kDa. Molecular weight markers are indicated on the right in kDa. Wb, Western blotting. (C and D) TAG-1 bead binding on NrCAM-expressing (C) or parental (D) B104 cells. Cells were incubated for 30 min with TAG-1 beads and fixed with 4% paraformaldehyde. (E) Quantitative analysis of TAG-1 and F3Fc bead binding on parental and NrCAM-expressing B104 cell lines. (F–H) B104 cells expressing the NrCAMΔfn construct tagged with GFP were incubated with soluble TAG-1IgFc chimera clustered with anti-Fc antibodies for 30 min. Binding sites for the TAG-1 chimera (F, red) were colocalized with the GFP fluorescence of NrCAMΔfn expressed at the cell membrane (G, green). Overlay image in H. Bars: 20 μm in C and D; 10 μm in F–H.

beads (70%, n = 80) moved rearward with a velocity of 1.5 ± 0.7 μm/min (n = 7) and rapidly became resistant to displacement with the laser trap (84%, n = 80; Figure 3A, Table 1), a behavior similar to that on cells expressing full-length NrCAM. Thus, deletion of the cytoplasmic tail did not impair the retrograde mobility of NrCAM and its tight coupling to the cytoskeleton.

Linkage with the Cytoplasmic Tail and cis-interaction through the FNIII Domains Independently Drive NrCAM Retrograde Mobility on the Cell Surface

Next, we made the hypothesis that NrCAM may associate in *cis* with transmembrane proteins via its extracellular domain when clustered by TAG-1 beads. Binding experiments with

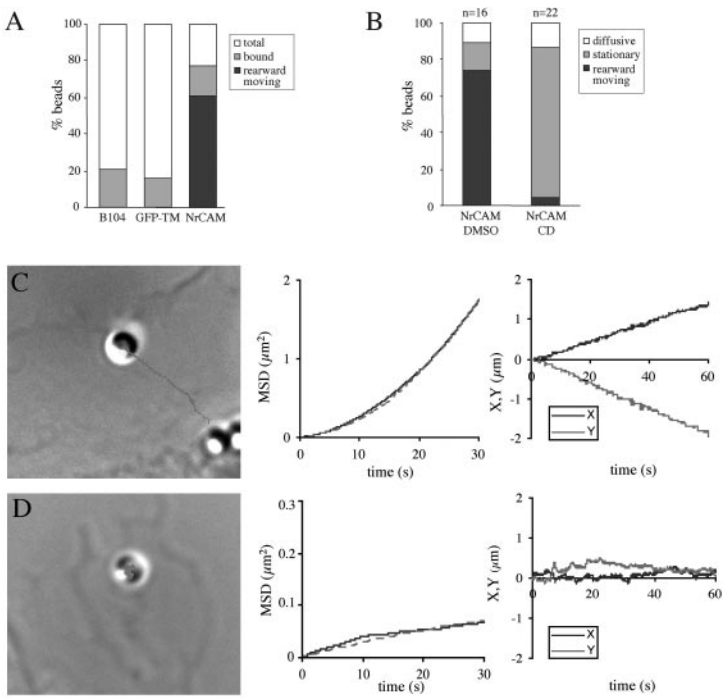

Figure 2. Actin-dependent retrograde mobility of TAG-1 beads on NrCAM-expressing B104 cells analyzed by single particle tracking. (A) Quantitative analysis of TAG-1 beads binding and rearward movement on parental, GFP-TM-, or NrCAM-expressing B104 cells. (B) TAG-1 bead mobility analyzed by time-lapse recording on NrCAM-expressing cells treated for 15 min with DMSO or 2 μM cytochalasin D (CD). (C) Representative trajectory of a TAG-1 bead placed onto NrCAM-expressing B104 cell with optical tweezers. The bead is shown at its original position, at the periphery of the lamellipodium. The trajectory was calculated from the time-lapse recording during a 60-s period. The mean squared displacement (MSD) plotted as a function of time interval (plain line) follows a parabolic curve (dashed line) characteristic of a unidirectional diffusion mode as indicated by the directional velocity V = 2.5 μm/min and diffusion coefficient D = 1.3 10^{-3} μm^2 s^{-1}. Plots of *X* and *Y* coordinates vs. time show a uniform bead movement away from the leading edge. (D) NrCAM-expressing cell treated with 2 μM cytochalasin D for 15 min before time-lapse recording. The bead showed a stationary behavior. V = 0.3 μm/min and D = 0.3 10^{-3} μm^2 s^{-1} were calculated from the MSD curve (note that the *Y*-axis scale of the MSD curve differs from C). *X* and *Y* coordinates showed very slight variations vs. time.

soluble NrCAMFc preclustered with anti-Fc indicated that NrCAM binding sites were indeed present at the surface of B104 cells (unpublished data). Such *cis*-interacting molecules may provide an indirect linkage between NrCAM and the cytoskeleton. We hypothesized that NrCAM may be engaged in a *cis*-interaction via its FNIII domains, triggered by *trans*-interaction of the Ig domains with TAG-1 beads. To test this hypothesis, we generated a NrCAM construct in which the four FNIII domains were replaced by GFP (NrCAMΔfn; Figure 1A). As shown in Figure 3A, deletion of the FNIII domains did not impair NrCAM anchorage to the cytoskeleton. Indeed the major part of TAG-1 beads (72%, n = 36) moved rearward shortly after their attachment to the cell surface and could not be recaptured by the laser trap (Figure 3A, Table 1). Thus, FNIII domains seemed to be dispensable for the coupling of NrCAM to the retrograde actin flow.

We then generated a construct with deletions of both the FNIII domains and the cytoplasmic tail (NrCAMΔfnΔcyt).

Table 1. Movement of TAG-1 beads on the various NrCAM-expressing clones

	Rearward moving			No rearward mobility			
	% Escaped initial trap	% Escaped retrapping	% Retrapped	% Escaped retrapping	% Retrapped	(n)	Mean coupling index
Coupling index	3	2	1	1	0		
NrCAM	20	50.8	9	9.2	10	(65)	1.80 ± 0.12
NrCAMΔcyt	17.5	45	7.5	12.5	17.5	(80)	1.56 ± 0.15
NrCAMΔfn	30.6	36.1	5.5	11.7	16.7	(36)	1.88 ± 0.18
NrCAMΔfnΔcyt$_1$[a]	5	5	15	30	45	(20)	0.78 ± 0.18[b]
NrCAMΔfnΔcyt$_2$[a]	1.7	8.3	18.3	23.4	48.3	(60)	0.67 ± 0.13[b]
NrCAMΔfnΔCter	0	12.5	0	59.4	28.1	(32)	0.84 ± 0.11[b]
NrCAM/CD	0	4.3	0	73.9	21.7	(23)	0.82 ± 0.10[b]
NrCAM/MBCD	0	18.7	6.3	62.5	12.5	(16)	1.01 ± 0.14[b]
NrCAM/DMSO	25	37.5	6.3	18.7	12.5	(16)	1.75 ± 0.25

Initial attachment of beads was induced for a 5-s period with the laser trap in the peripheral region of lamellipodia. Beads that displayed a directional movement toward the proximal region of the lamellipodia (velocity >1 μm/min) were scored as rearward moving. Beads that escaped the trap during the attachment period always displayed a rearward mobility and were scored as "escaped initial trap." Following the period of trajectory recording, the resistance of beads to displacement with the laser trap was tested: beads were scored as "retrapped" when dragged by the laser trap or as "escaped the trap" when resisting the laser trapping. NrCAM-expressing cells were treated with DMSO, MBCD, or cytochalasin D (CD) for 15 min before laser trapping assays. (*n*) is the number of beads recorded. For statistical analysis, a coupling index was attributed for each bead behavior as indicated in the table.

[a] NrCAMΔfnΔcyt$_1$ and NrCAMΔfnΔcyt$_2$ correspond to two clones of stably transfected B104 cells.

[b] Indicates a significant difference ($p<0.01$) of the mean coupling index by comparison with full-length NrCAM using ANOVA.

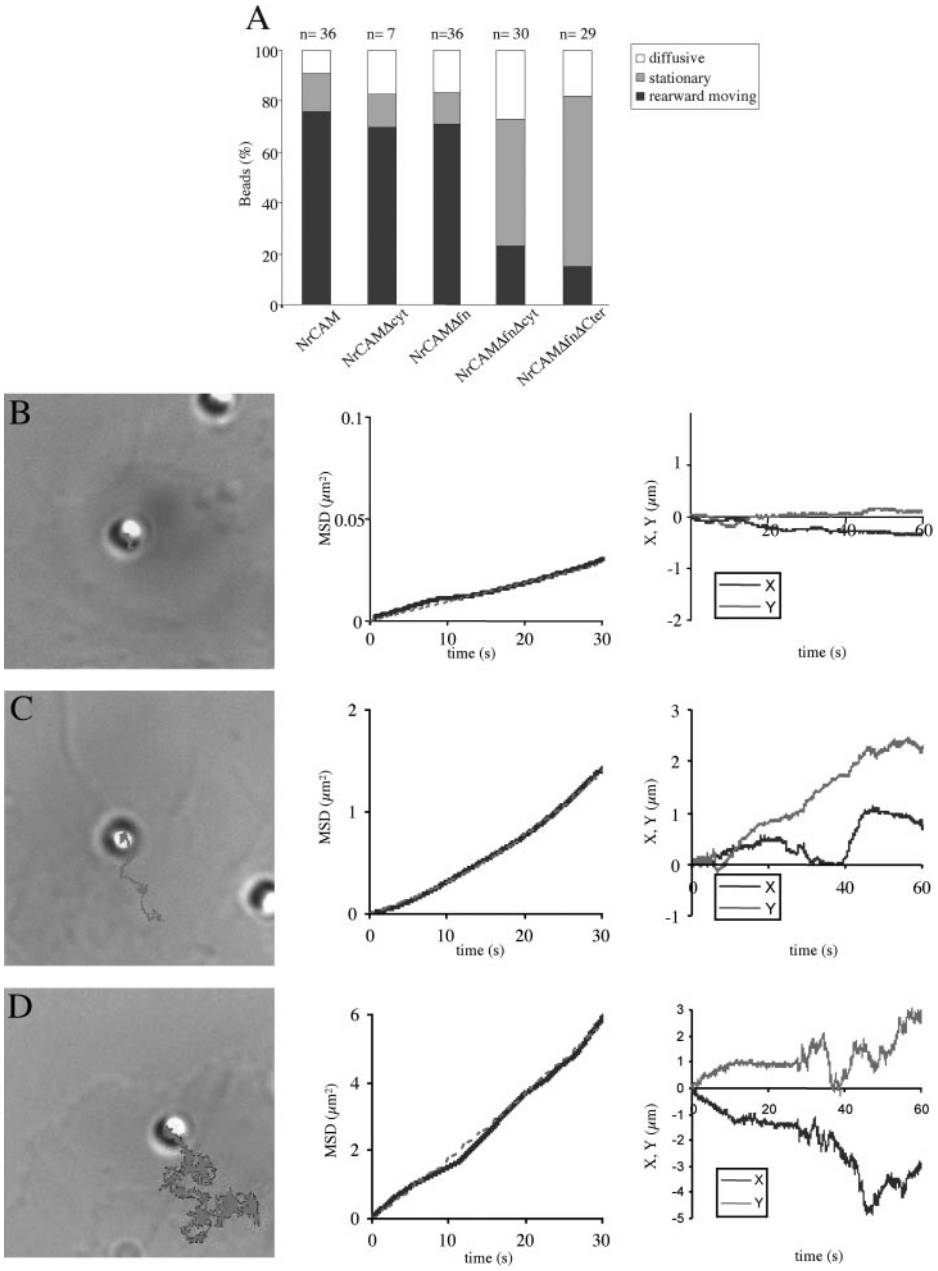

Figure 3. Behavior of TAG-1 beads on B104 cells expressing NrCAM-deleted constructs analyzed by single particle tracking and laser trapping experiments. (A) Quantitative analysis of TAG-1 bead mobility on B104 cells expressing NrCAM, NrCAMΔcyt, NrCAMΔfn, NrCAMΔfnΔcyt, and NrCAMΔfnΔCter. Bead movements were classified as "stationary" when displacement did not exceed 1 μm/min, otherwise as "diffusing" or "rearward moving." (B–D) Panels exemplifying the three types of TAG-1 bead behaviors on NrCAMΔfnΔcyt-expressing cells: stationary (B), rearward moving (C), and diffusive (D). The beads are shown at the initial attachment site, and the trajectory was deduced from the time-lapse recording during a 60-s period. MSD plotted as a function of time interval (plain line). Plots of *X* and *Y* coordinates vs. time. Note that *Y*-axis scales differ in B, C, and D. (B) Most TAG-1 beads exhibited a stationary behavior. Analysis of a representative trajectory showed a slow directional velocity V = 0.3 μm/min and a diffusion coefficient D = 0.8 10^{-3} μm^2 s^{-1}. (C) A low percentage of TAG-1 beads displayed a directed movement as indicated by the MSD plots vs. time (plain line), which followed a parabolic curve (dashed line). However, the trajectory was irregular as shown in the curves of *X* and *Y* coordinates vs. time (compare with Figure 2C for full-length NrCAM). (D) Some of the TAG-1 beads were mostly diffusive, as on this example with chaotic *X* and *Y* displacements vs. time. The MSD curve vs. time is in blue, and the red line reflect the best fit of this curve by linear regression and gives an average diffusion coefficient D = 1.3 ± 2.7 10^{-2} μm^2 s^{-1} (n = 14).

This construct was stably transfected into B104 cells and two clones were selected on the basis of their strong receptor expression at the cell surface as judged by Western blotting (Figure 1B). TAG-1 bead binding was observed to occur on NrCAMΔfnΔcyt-expressing cells (97%, n = 82) as on cells transfected with full-length NrCAM. In contrast with their behavior on clones expressing NrCAM constructs deleted of only their cytoplasmic tail or their FNIII domains, TAG-1 beads rarely moved rearward on NrCAMΔfnΔcyt-expressing clones (Figure 3). The percentage of beads displaying retrograde mobility was strongly reduced to 27% (vs. 80% in cells expressing full-length NrCAM; Table 1). It should be noted that the low percentage of TAG-1 beads that moved rearward adopted an irregular trajectory exhibiting temporary diffusion periods (Figure 3C). In addition, the percentage of TAG-1 beads that escaped to laser retrapping strongly decreased (33 vs. 80% for full-length NrCAM; Figure 3A, Table 1). Therefore the NrCAMΔfnΔcyt construct exhibited a reduced capability of anchorage to the cytoskeleton.

Surprisingly, only few of the nonrearward moving TAG-1 beads freely diffused on NrCAMΔfnΔcyt-expressing cells (27%, n = 30; Figure 3, A and D), as observed for TAG-1 beads that unspecifically attached on parental B104 cells. The major part of the nonrearward moving beads remained stationary during the 3-min recording period (50%, n = 30), as if they were confined to a specific domain of the lamellipodia (Figure 3B). Beads that were judged immobile by eye exhibited either a small directional movement or a complete immobility, resulting in a very low mean velocity 0.1 ± 0.2 μm/min (n = 9). However, despite this reduced mobility, a large percentage (64%) of the nonrearward-moving beads were displaced by the laser trap, indicating loose anchoring to the cytoskeleton.

A coupling index was attributed to the different NrCAM constructs, based on three parameters: escaping initial trap

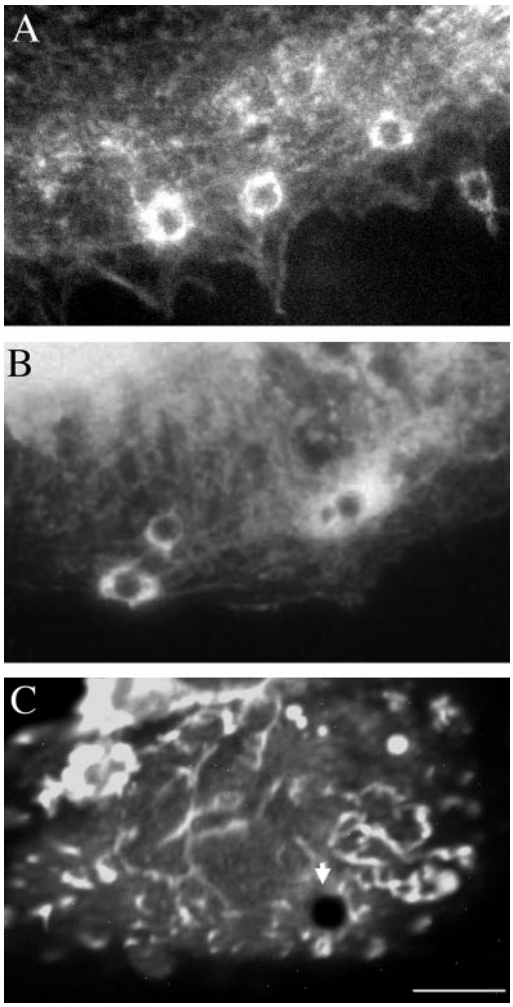

Figure 4. TAG-1 bead-mediated clustering of NrCAM induced the recruitment of F-actin and α-actinin at the bead-cell contact. NrCAM-expressing cells were incubated for 30 min with 4-μm TAG-1 beads. Cells were fixed with paraformaldehyde, permeabilized with Triton X-100 and processed for staining with Texas red–conjugated phalloidin (A) or immunofluorescence staining with anti-α-actinin (B) or anti-ezrin (C) antibodies. Actin filaments and α-actinin were heavily recruited at the contact site with TAG-1 beads. In contrast, ezrin did not appear to be concentrated at the TAG-1 bead contact (arrow). Bar, 12 μm.

before the 5-s period of bead attachment, rearward movement, and resistance to retrapping after bead attachment (Table 1). A statistical analysis was carried out to compare the coupling index of the different NrCAM constructs. Single deletions of the cytoplasmic tail or FNIII domains did not result in any significant alteration of the coupling with the cytoskeleton, whereas deletion of both regions had a significant effect (Table 1). Several conclusions can be drawn from the results with the NrCAMΔfnΔcyt construct. First, we can infer that in absence of the FNIII domains, the cytoplasmic tail is required for a direct coupling of NrCAM with the actin retrograde flow. Second, we can conclude that in absence of the cytoplasmic tail of NrCAM, the FNIII domains are implicated in the recruitment of NrCAM into a heterocomplex with a *cis* partner that provides an efficient anchorage to the actin cytoskeleton. Taken together, these data point to a role for the cytoplasmic tail of NrCAM in its coupling with the actin retrograde mobility, which should be reinforced by *cis*-association mediated by the FNIII region.

Role of the Cytoplasmic Domain of NrCAM in Its Coupling with the Actin Cytoskeleton

Next, we initiated mapping of the cytoplasmic region of NrCAM involved in the coupling with the F-actin retrograde flow. NrCAM is subject to extensive alternative splicing in six different regions of the extracellular domain, but also in the cytoplasmic region. Interestingly, a splicing variant has been characterized from human and chicken brain that displays a stop codon before the last 82 amino acids (Dry *et al.*, 2001). If translated, this mRNA would generate a NrCAM isoform lacking the highly conserved ankyrin-binding domain and the C-terminal PDZ-domain binding motif. We generated a NrCAM construct with a truncation of the last C-terminal 70 amino acids (NrCAMΔfnΔCter) that was stably transfected in B104 cells (Figure 1, A and B). Most of TAG-1 beads attached to the cell surface but did not display rearward movement (Table 1, Figure 3B), as also observed for the NrCAMΔfnΔcyt construct. This stationary behavior resulted in a low velocity of 0.2 ± 0.1 μm/min (n = 4). Thus, the C-terminal region is critically involved in receptor anchorage with the retrograde actin flow. However, the percentage of TAG-1 beads that resisted to displacement by the laser trap was estimated to 72 vs. 33% for the NrCAMΔfnΔcyt construct (Figure 3A), indicating that the 44 aa juxta-membrane region of the cytoplasmic tail may be implicated in interaction with the cytoskeleton. The juxta-membrane region is involved in the colocalization of L1 with actin stress fibers in transfected glioma cells and was proposed to potentially mediate interaction with α-actinin (Dahlin-Huppe *et al.*, 1997). In addition, the juxta-membrane region contains a consensus motif for the binding of FERM proteins (Hoover and Bryant, 2000).

Because both α-actinin and the FERM protein ezrin are present in the peripheral domain of lamellipodia, we examined the possibility of NrCAM association with these actin-binding proteins. Using long-term binding assays with 4-μm TAG-1 beads on NrCAM-expressing cells, we analyzed the distribution of both proteins and actin filaments by immunofluorescence. We observed that F-actin (Figure 4A) and α-actinin (Figure 4B) were both heavily recruited and colocalized at the site of bead-cell contact. In contrast, the ezrin-rich filopodial structures were found apposed to the TAG-1 beads, but ezrin did not appear to be recruited at the contact site (Figure 4C). The recruitment of α-actinin was observed at the contact for 36% (n = 209) of the beads attached to the lamellipodia of NrCAM-expressing cells. In addition, we tested the recruitment of other adaptors involved in the cytoskeletal linkage at adherent contacts. Talin, which has been implicated in the mechanical coupling between integrins and actin filaments (Giannone *et al.*, 2003), was not observed to be recruited under TAG-1 beads.

NrCAM Partitioning with Lipid Rafts

Laser-trapping experiments with TAG-1 beads indicated that clustered NrCAMΔfnΔcyt receptors displayed very reduced mobility in the absence of interactions with the cytoskeleton, suggesting that they were associated with membrane structures supporting confinement. We hypothesized that such reduced mobility might be due to the recruitment of clustered receptors into lipid rafts (Pralle *et al.*, 2000; Suzuki *et al.*, 2000; Tanimura *et al.*, 2003). Indeed, NrCAM contains a palmitoylation sequence in its *trans*-membrane domain that is conserved in the L1-family, and neurofascin has been reported to be palmitoylated at this site and to partition with lipid rafts (Ren and Bennett, 1998). Because

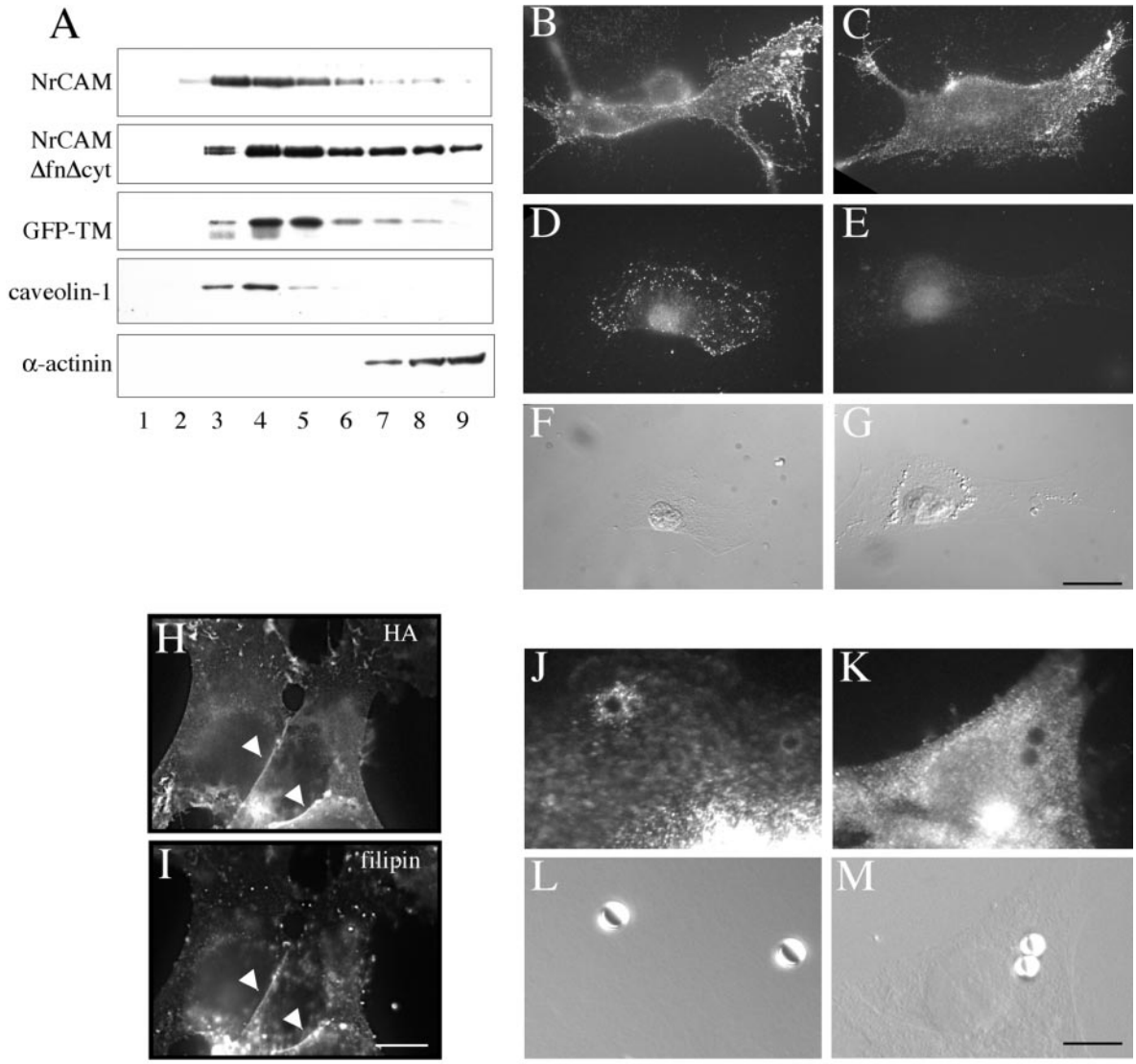

Figure 5. NrCAM partitioning with lipid rafts. (A) B104 cells expressing NrCAM, NrCAMΔfnΔcyt, or GFP-TM were lysed with 1% Lubrol and subjected to sucrose equilibrium gradients. The different fractions (numbered from top to bottom) were collected and analyzed by SDS-PAGE and Western blotting. Immunoblotting for caveolin-1 indicates that the low-density fractions 3–5 contained lipid rafts. In contrast, α-actinin was only detected in high-density fractions. NrCAM, NrCAMΔfnΔcyt, and GFP-TM were recovered in low-density fractions as analyzed by immunoblot with anti-HA mAb. (B–G) Triton X-100 extraction of NrCAMΔfnΔcyt in living cells is induced by treatment with MBCD. Live NrCAMΔfnΔcyt-expressing cells were immunostained with anti-GFP antibodies without (B) or with 0.1% Triton X-100 incubation for 3 min (D) before fixation with paraformaldehyde. A treatment with 10 mM MBCD for 30 min to deplete membrane cholesterol had no effect on NrCAM immunostaining (C), whereas it strongly reduced immunofluorescence for NrCAM after Triton X-100 extraction in living cells (E). (F and G) Nomarski images corresponding to D and E, respectively, showed that Triton X-100 extraction and MBCD treatment did not alter the flat cell morphology. Bar, 20 μm. (H and I) NrCAM-expressing cells were fixed with paraformaldehyde, permeabilized with Triton X-100, and immunostained with anti-HA antibodies (H) and incubated with 50 μg/ml filipin to fluorescently label the cholesterol (I). Note that filipin was colocalized with NrCAM enriched at the cell junctions (arrowheads). Bar, 20 μm. (J–M) NrCAMΔfnΔcyt-expressing cells were incubated for 30 min with 4 μm-beads coupled with TAG-1IgFc. Cells were fixed with paraformaldehyde, permeabilized with Triton X-100, and processed for immunofluorescence staining with anti-caveolin-1 antibody. A punctate staining for caveolin-1 was detected at the contact with TAG-1 bead (J and L). In control experiments, GFP-TM–expressing cells were incubated with TAG-1 beads. Caveolin-1 was not recruited at the contact with such nonspecifically bound TAG-1 beads (K and M). Bar, 10 μm.

NrCAM is Triton X-100 soluble in microsomes, we used Lubrol to test for the partitioning of NrCAM into detergent-resistant membranes. NrCAM- and NrCAMΔfnΔcyt-expressing cells were extracted with Lubrol and subjected to an equilibrium sucrose gradient centrifugation. Both molecules were present in the low-density lipid raft fraction and copartitioned with the raft component caveolin-1 (Figure 5A). In contrast, the cytoskeleton linker α-actinin was only recovered in the high-density fractions at the bottom of the gradient (Figure 5A). The partitioning of NrCAM into the lipid raft fraction was mediated by its transmembrane domain because the membrane-spanning domain of NrCAM alone fused with GFP as an extracellular region (GFP-TM) was also present in the raft fractions (Figure 5A).

We then analyzed the distribution of NrCAM after antibody- or TAG-1–mediated clustering at the cell surface and

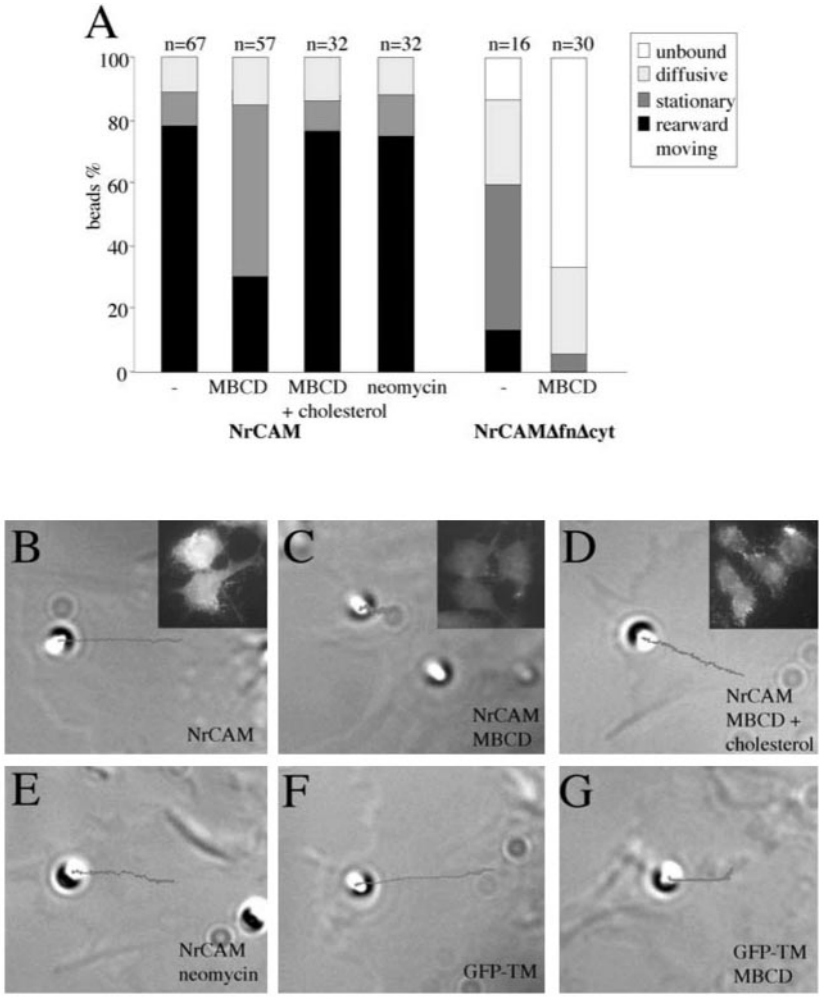

Figure 6. Raft dispersion using MBCD altered TAG-1 bead binding and mobility. (A) Single particle tracking analysis of TAG-1 bead mobility. Cells were incubated with 10 mM MBCD or with 10 mM MBCD saturated with cholesterol for 15 min before positioning beads with the laser trap. In NrCAM-expressing B104 cells, MBCD treatment had no effect on TAG-1 bead attachment but the major part of the beads became stationary. As controls, addition of MBCD saturated with cholesterol or 8-h treatment with 10 mM neomycin did not change the behavior of TAG-1 bead. In NrCAMΔfnΔcyt-expressing B104 cells treated with MBCD, a low percentage of beads attached to the cell membrane and displayed a diffusive behavior. (B–E) Examples of TAG-1 bead behaviors on NrCAM-expressing cells. Under control condition, the TAG-1 bead displayed a retrograde mobility ($V = 5.6\ \mu m$/min and $D = 6.3\ 10^{-3}\ \mu m^2\ s^{-1}$; B). A stationary behavior of TAG-1 beads was observed on cells treated with 10 mM MBCD (C). This representative trajectory showed a directional velocity $V = 0.7\ \mu m$/min and $D = 1.0\ 10^{-3}\ \mu m^2\ s^{-1}$. In the presence of 10 mM MBCD and 1.7 mM cholesterol, TAG-1 beads showed a retrograde mobility ($V = 3.9\ \mu m$/min and $D = 0.4\ 10^{-3}\ \mu m^2\ s^{-1}$; D). Insets show filipin staining to check that MBCD efficiently depleted cholesterol from NrCAM-expressing cells (C), whereas the staining was back to control levels (B) when MBCD was saturated with exogenous cholesterol (D). NrCAM-expressing cells were treated for 8 h with neomycin to alter PIP2 metabolism (E). This representative trajectory shows that neomycin did not block the rearward mobility of TAG-1 beads ($V = 2.7\ \mu m$/min and $D = 1.9\ 10^{-3}\ \mu m^2\ s^{-1}$). (F–G) Examples of con-A bead behaviors on GFP-TM-expressing cells. Under control condition, the con-A bead displayed rearward mobility ($V = 4.1\ \mu m$/min and $D = 8.0\ 10^{-3}\ \mu m^2\ s^{-1}$)(F). After MBCD treatment, the con-A bead showed a retrograde mobility ($V = 1.8\ \mu m$/min and $D = 0.8\ 10^{-3}\ \mu m^2\ s^{-1}$; G). The beads are shown at the initial attachment site and the trajectory was deduced from the time-lapse recording during a 60-s period. Directional velocities and diffusion coefficients were calculated from the MSD curves.

its resistance to Triton X-100 extraction in living cells. Both full-length NrCAM (unpublished data) and NrCAMΔfnΔcyt were detected in clusters that were resistant to Triton X-100 extraction (Figure 5, B, D and F). A treatment with MBCD to deplete membrane cholesterol did not modify cell surface expression (Figure 5C) but completely altered the resistance to Triton X-100 extraction of NrCAMΔfnΔcyt (Figure 5, E and G).

To further confirm the association of NrCAM with lipid rafts, coimmunofluorescence staining of NrCAM was carried out with filipin, a fluorescent molecule that is used to detect free cholesterol. As shown in Figure 5H, NrCAM, which mediated homophilic adhesion was highly concentrated at cell-cell contacts (arrowheads). Strikingly, intense filipin fluorescence was colocalized with NrCAM labeling at these contact sites (Figure 5I).

To determine whether the confined behavior of TAG-1 beads may result from the recruitment of NrCAMΔfnΔcyt into lipid rafts, we performed immunofluorescence stainings for caveolin-1. Caveolin-1 strongly accumulated at the contact site with TAG-1 beads (Figure 5, J and L). Quantitative analysis indicated that caveolin-1 was recruited under 32% of TAG-1 beads (n = 80). In contrast, caveolin-1 did not accumulate under TAG-1 beads nonspecifically bound to GFP-TM–expressing B104 cells (Figure 5, K and M). As a control, anti-Fc–coated beads very seldom bound to the cells and recruited neither NrCAMΔfnΔcyt nor caveolin-1 (unpublished data). This result demonstrates that a pool of raft-associated NrCAM is recruited by the binding of TAG-1 beads.

Lipid Raft Association Is Involved in NrCAM Coupling to the Cytoskeleton

MBCD treatment was further used to analyze the consequence of raft dispersion on TAG-1 bead attachment and rearward transport using laser tweezers experiments. B104 cells expressing full-length NrCAM or NrCAMΔfn were treated with MBCD for 15 min before positioning TAG-1 beads with the laser trap. The drug caused partial retraction of some cells, so we were careful to select only cells showing normal lamellipodial motility. The beads attached as in control conditions (100%) but only 30% displayed a rearward movement. Instead, most beads remained confined in the peripheral region of the lamellipodia and were resistant to displacement with the laser trap (62%, n = 16; Table 1, Figure 6, A and C). These confined beads had a mean velocity of $0.5 \pm 0.2\ \mu m$/min (n = 6). These results indicate that NrCAM is able to interact with immobile components of the cytoskeleton in a way independent from its partitioning with lipid rafts, but that its anchorage to the retrograde actin

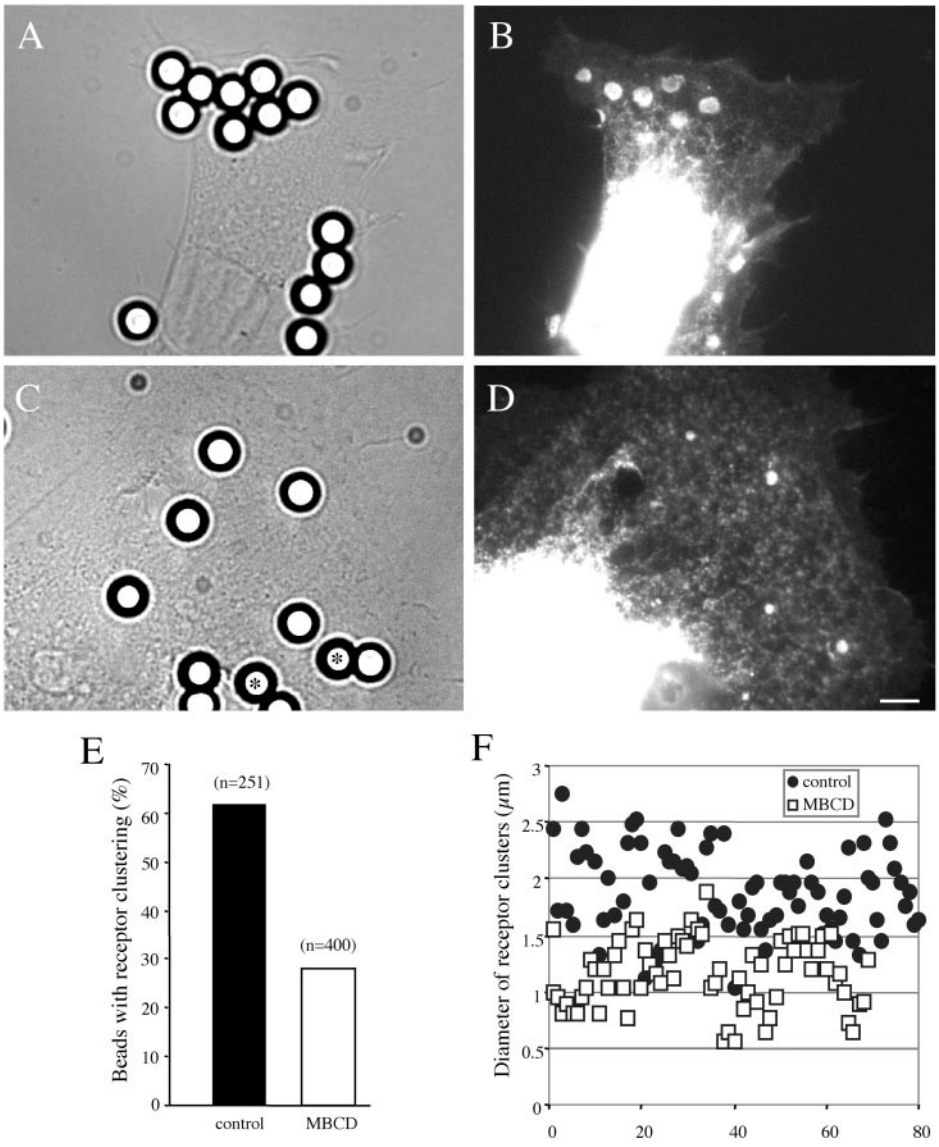

Figure 7. Raft dispersion using MBCD altered TAG-1 bead-mediated clustering of NrCAM. (A and D) NrCAMΔfnΔcyt-expressing cells were incubated for 15 min with 4-μm beads coupled with TAG-1IgFc and were treated or not with 10 mM MBCD for an additional 15 min. Then, cells were fixed with paraformaldehyde. Fluorescence imaging for GFP indicated a strong recruitment of GFP-tagged receptors that formed clusters at the bead-cell contacts under control condition (A and B). MBCD treatment resulted in the reduction of the size of GFP-clusters at cell-bead contacts and the GFP-cluster was even not detectable under some beads (asterisks; C and D). Bar, 5 μm. (E) Quantitative analysis of the percentage of beads that displayed a detectable GFP-cluster of NrCAM receptors under control condition or after MBCD treatment. (F) Individual diameters of the GFP-clusters were decreased after MBCD treatment when compared with the control. Statistical analysis using ANOVA indicated a significant effect ($p < 0.001$).

flow critically requires lipid raft integrity. Next, we analyzed the effect of MBCD treatment on cells expressing NrCAMΔfnΔcyt. TAG-1 beads that were maintained in contact with the cell surface during 5 s did not attach well and the low percentage of attached beads (35%) underwent long-range diffusion (85%, n = 7; Figure 6A).

Because the specificity of MBCD has been recently questioned (Edidin, 2003; Kwik *et al.*, 2003), we carried out a series of control experiments. First, MBCD saturated with exogenous cholesterol did not change the behavior of TAG-1 beads compared with that of untreated cells (Figure 6, A and D). Under this condition, TAG-1 beads displayed a rearward movement (78%, n = 32) with a mean velocity of 2.7 ± 0.3 μm/min (n = 10). Thus, the transition from retrograde to stationary behavior induced by MBCD was specific of cholesterol depletion. Second, because a recent study indicates that MBCD treatment perturbs the phosphoinositide metabolism, which in turn influences actin organization (Kwik *et al.*, 2003), control experiments were performed using neomycin sulfate to sequester membrane PI(4,5)P2. Cells were treated with 10 mM neomycin sulfate for 8 h because a longer treatment was toxic. After neomycin treatment, most TAG-1 beads displayed a rearward mobility with a mean velocity of 2.1 ± 0.3 μm/min (n = 8, Figure 6, A and E). Thus, neomycin did not block the rearward mobility of NrCAM. Third, beads coated with con-A were used to evaluate global effects of MBCD on lamellipodial actin flow (Suter *et al.*, 1998). To make sure that con-A would not attach to NrCAM, we used the clone GFP-TM. Con-A beads attached and displayed rearward mobility with a mean velocity of 4.3 ± 1.1 μm/min (n = 4, Figure 6F). After MBCD treatment, most con-A beads (76%, n = 17) still moved rearward, albeit with a slower velocity of 1.5 ± 0.7 μm/min (n = 5, Figure 6G). This indicates that MBCD reduces the speed of the cortical actin flow but does not affect the coupling of lectin receptors to it.

Lipid Raft Association Is Involved in Ligand Binding and Clustering of NrCAM

In a second step, we analyzed TAG-1 bead binding in long-term assays in the presence of MBCD. Cells were first treated with 10 mM MBCD for 30 min and incubated with 4-μm TAG-1 beads for 30 min. We observed 72 and 76% reduction of bead binding on cells expressing NrCAMΔcyt and

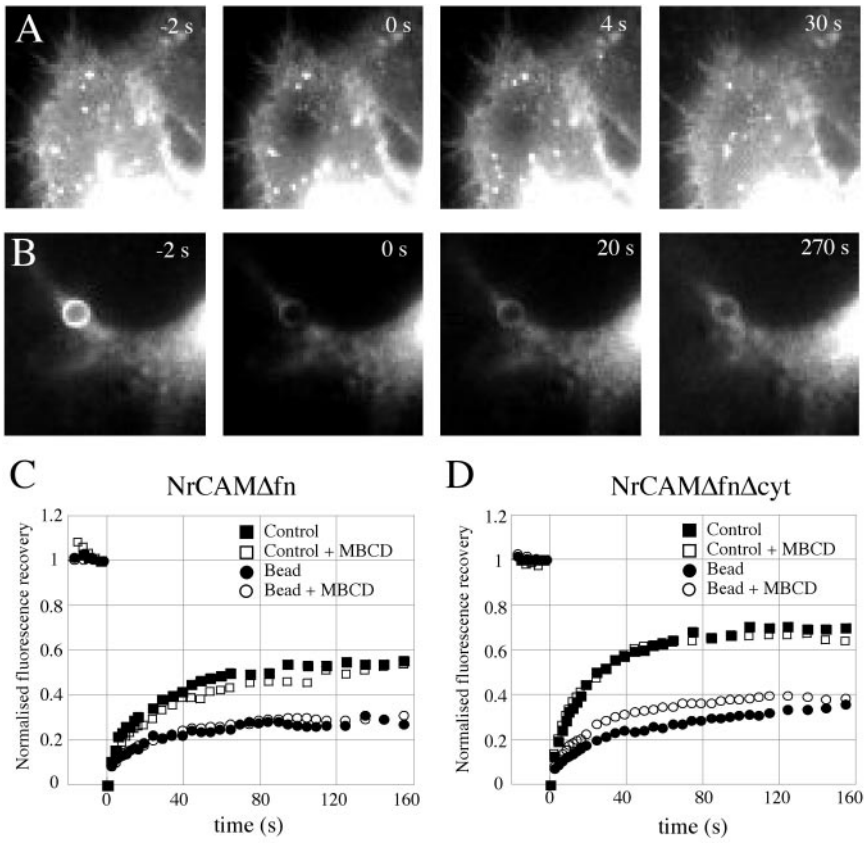

Figure 8. The effect of cholesterol depletion on the mobility of NrCAM analyzed by FRAP. Cells transfected with NrCAMΔfn (C) or NrCAMΔfnΔcyt (A, B, and D) were incubated for 20 min with 4-μm TAG-1 beads and then treated or not with 10 mM MBCD for 15 min. (A and B) Representative images of the FRAP sequence are shown for NrCAMΔfnΔcyt, and are similar to NrCAMΔfn. A 4-μm-diameter spot was photobleached in a region without a bead (A), or precisely on a bead-cell contact where the receptor is heavily clustered (B), and the fluorescence intensity was monitored. (C and D) Kinetics of the fluorescence recovery. Data are normalized to yield an intensity of zero immediately after photobleaching and represent the average of 6–12 individual traces. Plain curves are a fit through the data of the function $I_m^*(1 - \exp(-t/\tau))$, where I_m is the recovery fraction and τ a recovery time.

NrCAMΔfnΔcyt, respectively, after MBCD treatment. Binding of TAG-1 beads on full-length NrCAM-expressing cells was reduced by 53% in contrast with laser trapping assays in which forced interaction resulted in attachment of the beads in most of the trials. Because MBCD treatment did not reduce cell surface expression of NrCAM (Figure 5C), we hypothesize that under this experimental condition, lipid raft dispersion precluded the clustering of receptors, thus preventing efficient binding of the ligand.

To address this point, a quantitative analysis was performed to evaluate receptor clustering under control condition and after a brief MBCD treatment (Figure 7). Cells were first incubated with 4-μm TAG-1 beads for 15 min and then treated or not with 10 mM MBCD for 15 min. Under this experimental condition, the mean number of beads attached to the cell surface was not modified by MBCD treatment. The GFP-fluorescent clusters of NrCAMΔfnΔcyt at the bead-cell contacts displayed a mean diameter of 1.8 ± 0.4 μm (Figure 7, A, B, and F). After 15-min treatment with MBCD, this diameter was reduced to 1.2 ± 0.3 μm (Figure 7, C, D, and F) and clusters of receptors were only detected under 28% of TAG-1 beads (vs. 62% under control condition; Figure 5E). MBCD treatment also altered the recruitment of α-actinin at the contact with TAG-1 beads in NrCAM-expressing cells. Alpha-actinin was only detected under 13% of TAG-1 beads (n = 173), compared with 36% under control condition. Therefore, disruption of rafts by MBCD altered the clustering of NrCAM molecules and the recruitment of α-actinin under TAG-1 beads that may in turn impair anchoring to the retrograde actin flow.

Role of the Cytoplasmic Domain and Raft-Partitioning on the Mobility of NrCAM

Finally, we analyzed the effect of bead clustering and MBCD treatment on the lateral mobility of NrCAM, using FRAP on GFP-tagged NrCAMΔfn and NrCAMΔfnΔcyt clones. Cells were incubated with TAG-1 beads and then treated or not with MBCD. A single photobleach was applied in areas of contact with TAG-1 beads or on control lamellipodia, and the fluorescence recovery was monitored in the bleached spot (Figure 8, A and B). In control areas with unclustered receptors, NrCAMΔfn fluorescence reached a plateau of 54% of the prebleach value with a characteristic recovery time around 20 s (Figure 8C, n = 8). The NrCAMΔfnΔcyt construct exhibited a similar recovery time and a plateau value of 68% (Figure 8D, n = 5). Thus, deletion of the cytoplasmic tail mediating anchorage with the cytoskeleton slightly increased the mobile fraction of NrCAM. Treatment with MBCD had no effect for either construct, suggesting that lipid raft disruption did not affect the mobility of unclustered receptors. The recovery of NrCAM fluorescence was then monitored in regions of contact with TAG-1–coated beads, where receptors accumulated (Figure 8B). In these patched areas, the mobile fractions of NrCAMΔfn and NrCAMΔfnΔcyt were significantly reduced by almost a factor of two, indicating that receptors were being trapped by long-lasting interactions with TAG-1 ligands (Table 2). The recovery time of NrCAMΔfn in bead contacts was similar to that in control regions, indicating that the diffusion of mobile receptors was unaltered in these adhesive zones. Also, MBCD treatment did not affect the recovery time of NrCAMΔfn in bead areas, indicating that the mobility of the full-length protein was not sensitive to raft structure. Dele-

Table 2. Recovery of NrCAM-GFP fluorescence after photobleaching

	Region	MBCD treatment	Recovery fraction (%)	Recovery time (s)	n
NrCAMΔfn	Control	−	54 ± 6	16 ± 1	8
		+	52 ± 4	21 ± 1	6
	Bead	−	25 ± 3	16 ± 3	7
		+	25 ± 3	22 ± 3	12
NrCAMΔfnΔcyt	Control	−	68 ± 2	18 ± 3	5
		+	65 ± 5	14 ± 1	5
	Bead	−	38 ± 6	39 ± 6	12
		+	39 ± 4	21 ± 3	10

Parameters were deduced from exponential fits on FRAP curves through the data of the function $I_m*(1-\exp(-t/\tau))$, where I_m is the recovery fraction and τ a recovery time. Mean ± standard error and statistical analysis using the unpaired Student's *t* test. Upon bead clustering, the recovery fraction was significantly lowered for both NrCAMΔfn and NrCAMΔfnΔcyt ($p<0.005$), independently of the MBCD treatment. The recovery time for NrCAMΔfnΔcyt at the bead contact was significantly lowered after treatment with MBCD ($p<0.05$). (*n*) is the number of experiments.

tion of the cytoplasmic tail slightly increased the mobile fraction of NrCAMΔfnΔcyt in the area of bead contact, as observed for the unclustered receptor. Interestingly, the recovery time was increased at the bead contact, showing that the unbound NrCAMΔfnΔcyt under the bead has a reduced mobility due to a bead-mediated clustering of the receptor. This could be due to either free NrCAM corecruitment with the ligand-engaged receptors in merged rafts or to transient interactions of unbound NrCAM with the raft. Indeed MBCD treatment significantly decreased this recovery time to the value of the unclustered receptor (Figure 8D, Table 2). All together, these results suggest that when NrCAM receptors are clustered upon TAG-1 binding, both the coalescence of rafts and anchorage with the cytoskeleton via the cytoplasmic tail are induced and result in lower receptor mobile fraction and/or diffusion coefficient.

DISCUSSION

The control of growth cone motility by cell-cell contacts is based on the assembly of adhesion complexes and the coupling of membrane receptors with the underlying actin cytoskeleton, to generate driving forces. Using optical tweezers and single particle tracking of beads coated with TAG-1 ligands, we have analyzed the mobility of NrCAM and its coupling to the actin cytoskeleton in neuroblastoma cells. We present evidence that several stages of interactions are implicated in the linkage of NrCAM to the retrograde actin flow. First, *cis*-interaction with the FNIII domains of NrCAM and association with the cytoplasmic tail independently lead to anchoring with the F-actin retrograde flow; second, the recruitment of NrCAM into lipid rafts is required for ligand binding and rearward movement of NrCAM. We show that several mechanisms for NrCAM clustering may cooperate: *trans*-interaction with the ligand is favored by raft partitioning and reciprocally, ligand binding induces raft merging.

Complex Interactions via the FNIII Domains and the Cytoplasmic Tail Mediate Coupling of NrCAM with the F-actin Retrograde Flow

Using TAG-1 beads, we induced both ligand occupancy and receptor clustering resulting in anchoring of NrCAM with the retrograde actin flow. TAG-1 beads escaped the trap during the attachment period with no possible retrapping, reminiscent of N-cadherin–coated beads on N-cadherin–expressing myogenic cells (Lambert *et al.*, 2002). This behavior is indicative of a strong and immediate coupling to the cytoskeleton, at variance with that of integrins showing progressive reinforcement of their linkage to the cytoskeleton when force is applied to them via fibronectin-coated beads (Choquet *et al.*, 1997). This suggests that the various families of adhesion receptors exhibit different physical coupling to the cytoskeleton, in agreement with their different cytosolic adaptors and transductory pathways.

We observed that deletion of the single cytoplasmic tail was not sufficient to abrogate the rearward movement of NrCAM triggered by TAG-1 beads. Our results indicate that TAG-1 binding may induce the recruitment of a transmembrane adaptor via a *cis*-interaction mediated by the FNIII domains of NrCAM. It is of particular interest to note that the third FNIII domain of the related L1-molecule homomultimerizes and supports RGD-independent interactions with several integrins (Silletti *et al.*, 2000). Additional work is needed to determine whether integrins may act as adaptors implicated in the coupling of NrCAM to the actin cytoskeleton.

On the other hand, deletion of the FNIII domains unmasked the role of the cytoplasmic tail in the rearward movement of the molecule and allowed to initiate mapping of the cytoplasmic motifs involved. Deletion of the last 70 aa at the C-terminus suppressed the receptor coupling with the F-actin retrograde flow, but not its anchoring to the cytoskeleton. We can conclude that the juxta-membrane region at least supports interaction with static components of the cytoskeleton and that the C-terminal region comprising the FIGQY ankyrin-binding site and SFV PDZ-protein binding sequence is required for the coupling with the retrograde actin flow (Figure 9). It has been reported that ankyrin binding on the FIGQY motif of L1 mediates rearward movement during initiation of neurites (Nishimura *et al.*, 2003). In another study, however, ankyrin binding was shown to induce rather a stationary behavior (Gil *et al.*, 2003). Alternatively, the C-terminal PDZ-binding domain may participate to the coupling of NrCAM with the retrograde actin flow.

In addition, we showed that α-actinin is recruited together with F-actin at the cell contact with TAG-1 beads, whereas ezrin and talin are not. Because α-actinin is implicated in the cross-linking of actin filaments and in their anchorage at focal contacts (Liu *et al.*, 2000), it may participate to the linkage of NrCAM with F-actin.

Role of Lipid Rafts in NrCAM Reduced Mobility

We showed that NrCAM, which contains a palmitoylation motif in its membrane-spanning domain, partitions into lipid rafts. Lipid rafts are probably very small (50 nm or below) and dynamic entities that are difficult to observe individually (Pralle *et al.*, 2000; Edidin, 2003). Only when their structural components are clustered can they be identified by light microscopy. Here, we showed by filipin staining the colocalization of NrCAM with cholesterol-rich domains at cell-cell contacts and the recruitment of the raft component caveolin-1 at the adhesive contact between the cell surface and TAG-1 beads. These data suggest that cross-linking of NrCAM by *trans*-interaction with TAG-1 induces the formation of patches enriched in lipid rafts that can be visualized by immunofluorescence. Reciprocally, we showed that raft-association of NrCAM is crucial for its clustering upon ligand binding. Cholesterol depletion induced by MBCD strongly reduced TAG-1 bead binding on

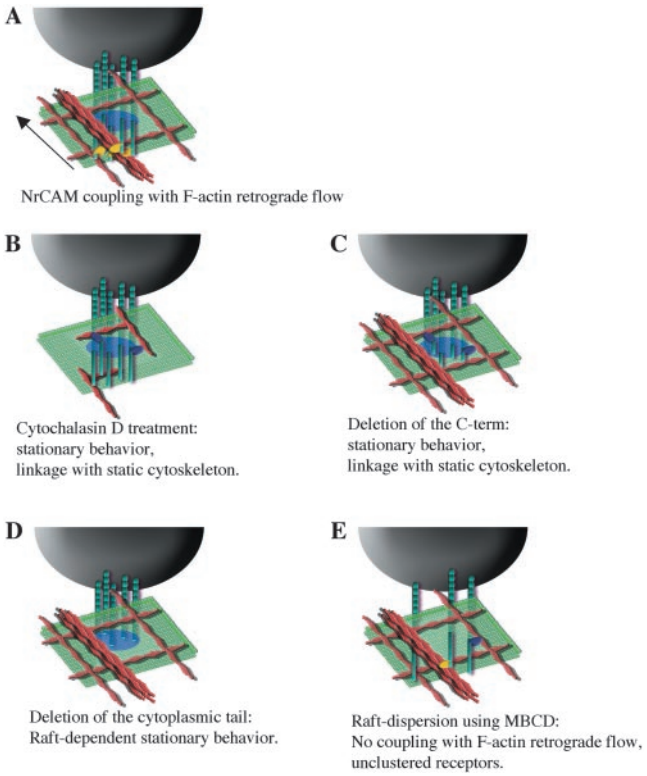

Figure 9. Models for NrCAM mobility in the cell membrane modulated through interactions with the cytoplasmic region and raft-partitioning. TAG-1 beads (black) bind NrCAM receptors (green). Patches of receptors are stabilized within lipid rafts (blue circle on the membrane) and the cytoplasmic tail interacts with the actin cytoskeleton (red) via adaptors (yellow or blue). (A) Retrograde mobility of the TAG-1 bead under control condition. The bead recruits a high density of NrCAM receptors. Under the bead, NrCAM cytoplasmic domains are associated to rearward flowing actin filaments. This coupling occurs via unknown adaptors (yellow). (B) TAG-1 bead on NrCAM after cytochalasin D treatment. Actin bund-les are depolymerized. NrCAM coupling to remnant subcortical cytoskeletal network may account for the limited mobility of the bead. (C) Stationary behavior on NrCAMΔfnΔCter. TAG-1 bead is resistant to displacement by the laser trap. The C-terminal part of the NrCAM cytoplasmic tail is required for the coupling with the actin retrograde flow. In this condition, the highly reduced mobility of the bead may reflect the linkage of the proximal region of the cytoplamic tail to static subcortical actin filaments via adaptors (blue). (D) TAG-1 bead on NrCAMΔfnΔcyt. NrCAM is unable to interact directly to the cytoskeleton. The bead displays a reduced mobility and can be displaced by the laser trap. This immobile behavior altered by MBCD treatment, depends on the partitioning of NrCAM within a bead-induced stabilized raft. (E) TAG-1 bead on NrCAM after MBCD treatment. Coupling of NrCAM with the actin retrograde flow is prevented. The bead displays a stationary behavior and resists to the laser trap displacement. Disruption of rafts by MBCD impairs NrCAM clustering and the receptor avidity for its ligand is reduced. The density of NrCAM molecules under the bead may be too low to permit clutching with the actin retrograde flowing. The stationary behavior is due to interaction of the cytoplasmic tail with the subcortical actin.

NrCAM-expressing cells, indicating that aggregation of NrCAM mediated by lipid rafts may increase the receptor avidity for its ligand. Organization of small receptor aggregates before ligand binding and rapid coalescence of individual rafts into large rafts upon ligand binding could account for the raft promotion of receptor clustering (Harris and Siu, 2002).

Upon clustering with TAG-1 beads, the NrCAMΔfnΔcyt receptors were not anchored to the F-actin retrograde flow and could be displaced by the laser trap, indicating a weak coupling to the cytoskeleton. However, the truncated receptors exhibited a stationary behavior in the cell membrane that was altered by MBCD treatment (Figure 9). Indeed, raft-associated proteins undergo abnormal diffusion, often exhibiting transient confinement (Sheets *et al.*, 1997; Simson *et al.*, 1998). In agreement with our results, microbeads attached to GPI-anchored proteins have a reduced diffusion coefficient, highly dependent on ligand density and area of the bead contact (Suzuki *et al.*, 2000). Other experiments using FRAP suggested that the decreased mobility of NrCAMΔfnΔcyt receptors observed in clusters was dependent on raft organization. Such mobility changes correlated with raft clustering have been observed for transmembrane proteins such HA (Shvartsman *et al.*, 2003) or the palmitoylated LAT adaptor upon T-cell activation (Tanimura *et al.*, 2003). Our data also illustrate that there seems to be a limited exchange of NrCAM between stabilized rafts under the bead and the surrounding plasma membrane, as inferred by local measurements of membrane viscosity using small beads coupled to raft-associated receptors (Pralle *et al.*, 2000).

Raft Partitioning Is Required for the Coupling of NrCAM with the Cytoskeleton

We have shown that raft dispersion using MBCD treatment abrogates NrCAM translocation with the F-actin retrograde flow. This might be due to MBCD-induced global modification of membrane properties and cytoskeletal organization. First, we checked that membrane expression of NrCAM was not changed after MBCD treatment in contrast to the diminution of several raft-associated proteins after long lasting LDL depletion (Sheets *et al.*, 1997). Second, MBCD treatment has been shown to decrease the lateral mobility of membrane receptors in FRAP analyses (Kenworthy *et al.*, 2004), which was correlated to a PIP_2-dependent cortical redistribution of F-actin (Kwik *et al.*, 2003). In contrast, our FRAP analyses showed no diminution in the mobility of unclustered NrCAM after MBCD treatment. In addition, NrCAM coupling with the F-actin retrograde flow was unaffected by neomycin, a drug that alters PIP2 metabolism. Moreover, because con-A beads still exhibited significant rearward movement after MBCD treatment, we assume that alteration of F-actin dynamics could not account for our results. Thus, the effect of MBCD was assessed to be specific because several drawbacks of cholesterol depletion protocols can be excluded in our study.

A high density of ligand coated on the bead surface is required for generating rearward movement of different types of receptors (Thoumine and Meister, 2000; Coussen *et al.*, 2002; Lambert *et al.*, 2002; Gil *et al.*, 2003). Beads inducing strong cross-linking exhibit a robust coupling with the actin cytoskeleton, and instead beads having lower cross-linking activity attach to the cell surface, but display loose cytoskeletal interactions. Reciprocally, we can assume that the raft-mediated packing of receptors is required for their strong coupling with the actin cytoskeleton (Figure 9). Indeed, we showed that MBCD-induced raft disruption alters NrCAM clustering and α-actinin recruitment at the contact with TAG-1 beads.

Alternatively, raft partitioning should enhance NrCAM-cytoskeleton interactions by selectively concentrating adaptors and making them readily available. Formation of enlarged rafts after cell aggregate formation has been shown to induce specific interactions with the cytoskeleton and to activate specific signaling pathways in *Dyctostelium* or at the

immunological synapse (Moran and Miceli, 1998; Harris and Siu, 2002). For example, recruitment into lipid rafts can induce association with the cortical actin cytoskeleton mediated by caveolin-1 or annexin II (Oliferenko *et al.*, 1999; Kanzaki and Pessin, 2002). In addition, rafts that consist in highly organized signaling platforms could be important for the F-actin clutching at adhesive contacts because this process requires highly regulated phophorylation-based signaling (Suter and Forscher, 2001; von Wichert *et al.*, 2003).

Finally, raft partitioning of NrCAM, which is implicated both in ligand-binding and rearward movement of the receptor, may be critical for the control of axonal growth. Indeed, recent studies indicate that the recruitment of CAMs into lipid rafts is involved in growth cone motility and axogenesis. For example, raft-exclusion of NCAM140 by mutation of its palmitoylation site impairs homophilic-mediated neurite outgrowth (Niethammer *et al.*, 2002). Furthermore, micro-CALI-mediated disruption of rafts slows the L1-dependent migration of DRG sensory neurons (Nakai and Kamiguchi, 2002). Interestingly, disruption of rafts in the peripheral domain, but not in the central domain affects growth cone migration. The peripheral domain is the region where clustering of the L1-molecule triggers anchoring with the F-actin retrograde flow to generate a tension force pulling the growth cone forward, and we demonstrated here that this process requires the integrity of rafts. More generally, it seems that lipid rafts play a pivotal role in the control of axonal guidance because raft-dependent signaling also mediates growth cone turning in response to chemotropic factors (Guirland *et al.*, 2004).

Multiple direct as well as indirect interactions of NrCAM with the actin cytoskeleton may provide a range of modulations of receptor mobility and ability to transduce mechanical forces. Having different possibilities of switching between static adhesion and dynamic coupling may be a key factor to allow a fine control of growth cone motility by addition of different regulatory interactions. Moreover, *cis*-interaction and raft association would probably allow integration of different environmental cues and coordination of several adhesive events.

ACKNOWLEDGMENTS

We thank André Le Bivic, Paul Mangeat, Marianne Renner, and Francis Chaouloff for helpful discussions. This work was supported by the Association pour la Recherche sur la Sclérose en Plaques, the Mizutani Foundation for Glycosciences, the Fondation pour la Recherche Médicale (C.F.-S.), and the Conseil Régional d'Aquitaine (D.C.).

REFERENCES

Bennett, V., and Chen, L. (2001). Ankyrins and cellular targeting of diverse membrane proteins to physiological sites. Curr. Opin. Cell Biol. *13*, 61–67.

Brümmendorf, T., and Rathjen, F.G. (1996). Structure/function relationships of axon-associated adhesion receptors of the immunoglobulin superfamily. Curr. Opin. Neurobiol. *6*, 584–593.

Choquet, D., Felsenfeld, D.P., and Sheetz, M.P. (1997). Extracellular matrix rigidity causes strengthening of integrin-cytoskeleton linkages. Cell *88*, 39–48.

Coussen, F., Choquet, D., Sheetz, M.P., and Erickson, H.P. (2002). Trimers of the fibronectin cell adhesion domain localize to actin filament bundles and undergo rearward translocation. J. Cell Sci. *115*, 2581–2590.

Dahlin-Huppe, K., Berglund, E.O., Ranscht, B., and W.B. Stallcup. (1997). Mutational analysis of the L1 neuronal cell adhesion molecule identifies membrane-proximal amino acids of the cytoplasmic domain that are required for cytoskeletal anchorage. Mol. Cell Neurosci. *9*, 144–156.

Davis, J.Q., Lambert, S., and Bennett, V. (1996). Molecular composition of the node of Ranvier: identification of ankyrin-binding cell adhesion molecules neurofascin (mucin+/third FNIII domain-) and NrCAM at nodal axon segments. J. Cell Biol. *135*, 1355–1367.

Dry, K., Kenwrick, S., Rosenthal, A., and Platzer, M. (2001). The complete sequence of the human locus for NgCAM-related cell adhesion molecule reveals a novel alternative exon in chick and man and conserved genomic organization for the L1 subfamily. Gene *273*, 115–122.

Edidin, M. (2003). The state of lipid rafts: from model membranes to cells. Annu. Rev. Biophys. Biomol. Struct. *32*, 257–283.

Faivre-Sarrailh, C., Falk, J., Pollerberg, E., Schachner, M., and Rougon, G. (1999). NrCAM, cerebellar granule cell receptor for the neuronal adhesion molecule F3, displays an actin-dependent mobility in growth cones. J. Cell Sci. *112*, 3015–3027.

Faivre-Sarrailh, C., Gauthier, F., Denisenko-Nehrbass, N., Le Bivic, A., Rougon, G., and Girault, J.A. (2000). The glycosylphosphatidyl inositol-anchored adhesion molecule F3/contactin is required for surface transport of paranodin/contactin-associated protein (caspr). J. Cell Biol. *149*, 491–502.

Falk, J., Bonnon, C., Girault, J.A., and Faivre-Sarrailh, C. (2002). F3/contactin, a neuronal cell adhesion molecule implicated in axogenesis and myelination. Biol. Cell *94*, 327–334.

Garver, T.D., Ren, Q., Tuvia, S., and Bennett, V. (1997). Tyrosine phosphorylation at a site highly conserved in the L1 family of cell adhesion molecules abolishes ankyrin binding and increases lateral mobility of neurofascin. J. Cell Biol. *137*, 703–714.

Giannone, G., Jiang, G., Sutton, D.H., Critchley, D.R., and Sheetz, M.P. (2003). Talin1 is critical for force-dependent reinforcement of initial integrin-cytoskeleton bonds but not tyrosine kinase activation. J. Cell Biol. *163*, 409–419.

Gil, O.D., Sakurai, T., Bradley, A.E., Fink, M.Y., Cassella, M.R., Kuo, J.A., and Felsenfeld, D.P. (2003). Ankyrin binding mediates L1CAM interactions with static components of the cytoskeleton and inhibits retrograde movement of L1CAM on the cell surface. J. Cell Biol. *162*, 719–730.

Grabham, P.W., Foley, M., Umeojiako, A., and Goldberg, D.J. (2000). Nerve growth factor stimulates coupling of beta1 integrin to distinct transport mechanisms in the filopodia of growth cones. J. Cell Sci. *113*, 3003–3012.

Guirland, C., Suzuki, S., Kojima, M., Lu, B., and Zheng, J.Q. (2004). Lipid rafts mediate chemotropic guidance of nerve growth cones. Neuron *42*, 51–62.

Harris, T.J., and Siu, C.H. (2002). Reciprocal raft-receptor interactions and the assembly of adhesion complexes. Bioessays *24*, 996–1003.

Hoover, K.B., and Bryant, P.J. (2000). The genetics of the protein 4.1 family: organizers of the membrane and cytoskeleton. Curr. Opin. Cell Biol. *12*, 229–234.

Jay, D.G. (2000). The clutch hypothesis revisited: ascribing the roles of actin-associated proteins in filopodial protrusion in the nerve growth cone. J. Neurobiol. *44*, 114–125.

Kamiguchi, H., and Yoshihara, F. (2001). The role of endocytic L1 trafficking in polarized adhesion and migration of nerve growth cones. J. Neurosci. *21*, 9194–9203.

Kanzaki, M., and Pessin, J.E. (2002). Caveolin-associated filamentous actin (Cav-actin) defines a novel F-actin structure in adipocytes. J. Biol. Chem. *277*, 25867–25869.

Kenworthy, A.K., Nichols, B.J., Remmert, C.L., Hendrix, G.M., Kumar, M., Zimmerberg, J., and Lippincott-Schawartz, J. (2004). Dynamics of putative raft-associated proteins at the cell surface. J. Cell Biol. *165*, 735–746.

Kunimoto, M. (1995). A neuron-specific isoform of brain ankyrin, 440-kD ankyrinB, is targeted to the axons of rat cerebellar neurons. J. Cell Biol. *131*, 1821–1829.

Kwik, J., Boyle, S., Fooksman, D., Margolis, L., Sheetz, M.P., and Edidin, M. (2003). Membrane cholesterol, lateral mobility, and the phosphatidylinositol 4,5-bisphosphate-dependent organization of cell actin. Proc. Natl. Acad. Sci. USA *100*, 13964–13969.

Lambert, M., Choquet, D., and Mege, R.M. (2002). Dynamics of ligand-induced, Rac1-dependent anchoring of cadherins to the actin cytoskeleton. J. Cell Biol. *157*, 469–479.

Lin, C.H., and Forscher, P. (1995). Growth cone advance is inversely proportional to retrograde F-actin flow. Neuron *14*, 763–771.

Liu, S., Calderwood, D.A., and Ginsberg, M.H. (2000). Integrin cytoplasmic domain-binding proteins. J. Cell Sci. *113*, 3563–3571.

Marchand, S., Devillers-Thiéry, A., Pons, S., Changeux, J.P., and Cartaud, J. (2002). Rapsyn escorts the nicotinic acetylcholine receptor along the exocytic pathway via association with lipid rafts. J. Neurosci. *22*, 8891–8901.

Moran, M., and Miceli, M.C. (1998). Engagement of GPI-linked CD48 contributes to TCR signals and cytoskeletal reorganization: a role for lipid rafts in T cell activation. Immunity *9*, 787–796.

Nakai, Y., and Kamiguchi, H. (2002). Migration of nerve growth cones requires detergent-resistant membranes in a spatially defined and substrate-dependent manner. J. Cell Biol. *159*, 1097–1108.

Niethammer, P., Delling, M., Sytnyk, V., Dityatev, A., Fukami, K., and Schachner, M. (2002). Cosignaling of NCAM via lipid rafts and the FGF receptor is required for neuritogenesis. J. Cell Biol. *157*, 521–532.

Nishimura, K., Yoshihara, F., Tojima, T., Ooashi, N., Yoon, W., Mikoshiba, K., Bennett, V., and Kamiguchi, H. (2003). L1-dependent neuritogenesis involves ankyrinB that mediates L1-CAM coupling with retrograde actin flow. J. Cell Biol. *163*, 1077–1088.

Oliferenko, S., Paiha, K., Harder, T., Gerke, V., Schwarzler, C., Schwarz, H., Beug, H., Gunthert, U., and Huber, L.A. (1999). Analysis of CD44-containing lipid rafts: recruitment of annexin II and stabilization by the actin cytoskeleton. J. Cell Biol. *146*, 843–854.

Pavlou, O., Theodorakis, K., Falk, J., Kutsche, M., Schachner, M., Faivre-Sarrailh, C., and Karagogeos, D. (2002). Analysis of interactions of the adhesion molecule TAG-1 and its domains with other immunoglobulin superfamily members. Mol. Cell Neurosci. *20*, 367–381.

Perrin, F.E., Rathjen, F.G., and Stoeckli, E.T. (2001). Distinct subpopulations of sensory afferents require F11 or axonin-1 for growth to their target layers within the spinal cord of the chick. Neuron *30*, 707–723.

Pralle, A., Keller, P., Florin, E.L., Simons, K., and Horber, J.K. (2000). Sphingolipid-cholesterol rafts diffuse as small entities in the plasma membrane of mammalian cells. J. Cell Biol. *148*, 997–1008.

Ren, Q., and Bennett, V. (1998). Palmitoylation of neurofascin at a site in the membrane-spanning domain highly conserved among the L1 family of cell adhesion molecules. J. Neurochem. *70*, 1839–1849.

Sakurai, T., Lustig, M., Nativ, M., Hemperly, J.J., Schlessinger, J., Peles, E., and Grumet, M. (1997). Induction of neurite outgrowth through contactin and Nr-CAM by extracellular regions of glial receptor tyrosine phosphatase beta. J. Cell Biol. *136*, 907–918.

Sakurai, T. *et al.* (2001). Overlapping functions of the cell adhesion molecules Nr-CAM and L1 in cerebellar granule cell development. J. Cell Biol. *154*, 1259–1273.

Schmidt, C.E., Dai, J., Lauffenburger, D.A., Sheetz, M.P., and Horwitz, A.F. (1995). Integrin-cytoskeletal interactions in neuronal growth cones. J. Neurosci. *15*, 3400–3407.

Sheets, E.D., Lee, G.M., Simson, R., and Jacobson, K. (1997). Transient confinement of a glycosylphosphatidylinositol-anchored protein in the plasma membrane. Biochemistry *36*, 12449–12458.

Shvartsman, D.E., Kotler, M., Tall, R.D., Roth, M.G., and Henis, Y.I. (2003). Differently anchored influenza hemagglutinin mutants display distinct interaction dynamics with mutual rafts. J. Cell Biol. *163*, 879–888.

Silletti, S., Mei, F., Sheppard, D., and Montgomery, A.M. (2000). Plasmin-sensitive dibasic sequences in the third fibronectin-like domain of L1-cell adhesion molecule (CAM) facilitate homomultimerization and concomitant integrin recruitment. J. Cell Biol. *149*, 1485–1502.

Simson, R., Yang, B., Moore, S.E., Doherty, P., Walsh, F.S., and Jacobson, K.A. (1998). Structural mosaicism on the submicron scale in the plasma membrane. Biophys. J. *74*, 297–308.

Stoeckli, E.T., and Landmesser, L.T. (1995). Axonin-1, Nr-CAM, and Ng-CAM play different roles in the in vivo guidance of chick commissural neurons. Neuron *14*, 1165–1179.

Suter, D.M., and Forscher, P. (2001). Transmission of growth cone traction force through apCAM-cytoskeletal linkages is regulated by Src family tyrosine kinase activity. J. Cell Biol. *155*, 427–438.

Suter, D.M., Errante, L.D., Belotserkovsky, V., and Forscher, P. (1998). The Ig superfamily cell adhesion molecule, apCAM, mediates growth cone steering by substrate-cytoskeletal coupling. J. Cell Biol. *141*, 227–240.

Suzuki, K., Sterba, R.E., and Sheetz, M.P. (2000). Outer membrane monolayer domains from two-dimensional surface scanning resistance measurements. Biophys. J. *79*, 448–459.

Tanimura, N. *et al.* (2003). Dynamic changes in the mobility of LAT in aggregated lipid rafts upon T cell activation. J. Cell Biol. *160*, 125–135.

Thoumine, O., and Meister, J.J. (2000). A probabilistic model for ligand-cytoskeleton transmembrane adhesion: predicting the behavior of microspheres on the surface of migrating cells. J. Theor. Biol. *204*, 381–392.

Tsiotra, P.C., Theodorakis, K. Papamatheakis, J., and Karagogeos, D. (1996). The fibronectin domains of the neural adhesion molecule TAX-1 are necessary and sufficient for homophilic binding. J. Biol. Chem. *271*, 29216–29222.

Volkmer, H., Leuschner, R., Zacharias, U., and Rathjen, F.G. (1996). Neurofascin induces neurites by heterophilic interactions with axonal NrCAM while NrCAM requires F11 on the axonal surface to extend neurites. J. Cell Biol. *135*, 1059–1069.

von Wichert, G., Jiang, G., Kostic, A., De Vos, K., Sap, J., and Sheetz, M.P. (2003). RPTP-alpha acts as a transducer of mechanical force on alphav/beta3-integrin-cytoskeleton linkages. J. Cell Biol. *16*, 143–153.

Zacharias, U., Norenberg, U., and Rathjen, F.G. (1999). Functional interactions of the immunoglobulin superfamily member F11 are differentially regulated by the extracellular matrix proteins tenascin-R and tenascin-C. J. Biol. Chem. *274*, 24357–24365.